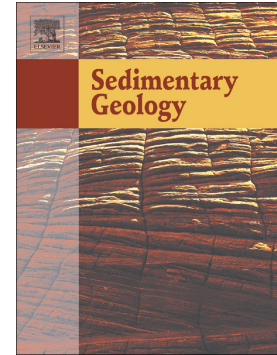


Journal Pre-proof

Particle size analysis: A comparison of laboratory-based techniques and their application to geoscience

J.E. Houghton, J. Behnsen, R.A. Duller, T.E. Nichols, R.H. Worden



PII: S0037-0738(24)00030-7

DOI: <https://doi.org/10.1016/j.sedgeo.2024.106607>

Reference: SEDGEO 106607

To appear in: *Sedimentary Geology*

Received date: 17 November 2023

Revised date: 14 February 2024

Accepted date: 15 February 2024

Please cite this article as: J.E. Houghton, J. Behnsen, R.A. Duller, et al., Particle size analysis: A comparison of laboratory-based techniques and their application to geoscience, *Sedimentary Geology* (2024), <https://doi.org/10.1016/j.sedgeo.2024.106607>

This is a PDF file of an article that has undergone enhancements after acceptance, such as the addition of a cover page and metadata, and formatting for readability, but it is not yet the definitive version of record. This version will undergo additional copyediting, typesetting and review before it is published in its final form, but we are providing this version to give early visibility of the article. Please note that, during the production process, errors may be discovered which could affect the content, and all legal disclaimers that apply to the journal pertain.

© 2024 The Author(s). Published by Elsevier B.V.

Particle size analysis: A comparison of laboratory-based techniques and their application to geoscience

J. E. Houghton¹, J. Behnsen², R. A. Duller¹, T. E. Nichols¹, & R. H. Worden^{1*}

¹Department of Earth, Ocean, and Ecological Science, University of Liverpool, Liverpool, L69 3GP, UK

²School of Engineering, University of Liverpool, Liverpool, L69 3GH, UK

*Corresponding author. Email address: r.worden@liverpool.ac.uk (R. H. Worden)

Abstract

In sedimentary geoscience, the particle size distribution (PSD) of a sediment has a fundamental effect on a sediment's ability to be entrained, eroded, and deposited. Therefore, it is crucial to accurately measure the PSD of sediments. Several laboratory-based methods of particle size analysis are commonly employed in geoscience; however, each method is based on different principles and the comparison of data from one technique to another is challenging. In this study, we have compared the output of four commonly-used laboratory-based techniques: Laser Particle Size Analysis (LPSA), optical point counting, 2D automated image analysis, and X-ray Computed Tomography (XCT). Each technique has been used to measure eight samples of spherical silica particles, all prepared with known particle size ranges. Spherical particles have been used to minimise the effects of variable sorting and particle shape on data output. Here we have compared the differences between the measured PSD and descriptors of each PSD, showing that, at small particle diameters (<150 μm), all techniques agree. However, at particle diameters >150 μm , LPSA overestimates the size of particles, due to limitations in the way that particle diameter is calculated by this technique. In contrast, 2D automated image analysis and optical point counting underestimate the diameters of particles, due to stereology (e.g., the effect of slicing particles during thin section preparation). Results from XCT analyses have the lowest values of sorting (range of measured particle diameters) and are therefore the most tightly constrained. In addition, XCT is the only 3D analysis method, allowing particle shape, orientation, and intraparticle porosity to be measured for a volume of material. We therefore conclude that XCT is the most accurate way to determine a grain size distribution in sediments.

Key words:

Particle size analysis; X-Ray Computed Tomography; Laser Particle Size analysis; Optical point counting; 2D automated image analysis

1. Introduction

Particle size and morphology are fundamental physical properties of sediment and sedimentary rocks that affect sediment erosion, transport, and deposition (Blott and Pye, 2001). Particle size analysis and the measured particle size distributions (PSD) therefore provide insights into sediment provenance and transport, and can allow for classification prediction and reconstruction of depositional environment (Folk and Ward, 1957; Friedman, 1979; Simon et al., 2021; Houghton et al., 2023). The PSD and particle morphology in sedimentary deposits also influence important physical properties of the sediment, such as porosity, permeability, load strength, and surface roughness (Beard and Weyl, 1973; Church, 1978; Blott and Pye, 2012). Particle size analysis has a range of applications outside of sedimentology that include: volcanology (Buckland et al., 2021), ceramics (Jillavenkatesa et al., 2001), additive manufacturing (Slotwinski et al., 2014; Behnsen et al., 2023), food processing (Devarrewaere et al., 2015), and pharmaceuticals (Gajjar et al., 2020). Therefore, understanding how laboratory-based methods of particle size analysis compare is valuable to a wide range of disciplines and users. This study aims to assess and compare laboratory-based methods of particle size analysis that are commonly used in the field of sedimentology, that include; optical point counting, 2D automated image analysis, Laser Particle Size Analysis (LPSA), and micro-focused X-ray Computed Tomography (XCT). Here we assessed the quantification of PSDs, inconsistencies associated with each method, and statistical descriptors of particle size for eight samples of spherical silica particles. We have also evaluated how results from the four techniques may be compared.

Use of the terminology surrounding particle size analysis (sometimes abbreviated to PSA) has been a long standing debate among geoscientists (Blott and Pye, 2012). The term “particle” was noted by Cadle (1965) to refer to an object of any size with defined physical boundaries in all directions. In geoscience, sediments can be individual particles (e.g., soil, dust, or sand particles) or assemblages of particles (e.g. clasts) (Blott and Pye, 2012). The size of a particle is a one-dimensional measurement of a length that is characteristic of the particle shape and volume. Particle size can be measured (e.g., maximum or minimum Feret diameters (Feret, 1930)), or calculated (e.g., equivalent circular diameter, or equivalent spherical diameter) (Figure 1). Particle size measurements are influenced, to varying extents, by particle shape, density, and optical properties. Therefore, the results from different particle size analysis techniques may not be directly comparable; making the comparison of PSD datasets challenging when multiple particle size analysis techniques are used (Pye, 1994). The particle size analysis methods used in this study, and the way in which a PSD was measured are discussed in section 2.

To obtain a statistically valid PSD in a geological sample, a minimum number of particles need to be counted. Van der Plas and Tobi (1965) studied the number of particles required to obtain representative mineralogy from optical point counting, and produced a chart to indicate the number of particles that require counting to achieve a given uncertainty. According to Mulholland and Jones (1968), estimation of mean particle size to within 0.1 phi, with 90% accuracy, requires 270 particles to be measured for a poorly sorted sandstone, and fewer particles are required for sandstones that are moderately to well sorted. Phi is a dimensionless unit of particle size measurement. A conversion between millimetres and phi was presented by Krumbein (1938), where ϕ is the particle diameter in phi units, and D is the particle diameter in millimeters:

$$\phi = -\log_2 D \quad (1)$$

Recent studies have suggested that counting between 100 and 400 particles, depending on statistical requirements, is sufficient to obtain representative descriptors from a sediment sample (Church et al., 1987; Fripp and Diplas, 1993; Rice and Church, 1996).

Statistical measurements, or descriptors, such as mean particle size and particle sorting, can be calculated from a PSD. Statistical measurements are regularly used to compare samples in the field of reservoir quality analysis (Ali et al., 2010), discrimination of sediment origin (Mason and Folk, 1958; Friedman, 1961), or to classify sedimentary sub-environment (Simon et al., 2021). The most useful PSD descriptors to identify trends in sediments have been reported to be mean particle size, modal particle size, and particle sorting (Folk, 1966). In contrast, it has been suggested that kurtosis is not a useful particle size descriptor (Folk, 1966).

The analysis of PSD data typically involves dividing a sample into a number of particle size bins, from which a PSD curve (or histogram) can be plotted using the sample mass, volumetric fraction, or percentage of the sample that lies within each particle size bin (Blott and Pye, 2001). Each particle size analysis technique produces data in a different manner, and it therefore remains the user's responsibility to interpret the results of particle size analysis appropriately, especially when comparing data from different methods (Blott and Pye, 2001). Particle size analysis has a wide range of applications within geoscience and therefore it is vital to understand how each method calculates a PSD, and how the resulting PSD from each method can be compared.

Using the measured PSD and calculated PSD descriptors, we compare for the first time, four independent laboratory-based particle size analysis techniques against a particle size range determined by sieving: Laser Particle Size Analysis (referred to as LPSA), 2D automated image analysis, optical point counting, and X-ray computed tomography (referred to XCT). Using a range of samples that vary in particle sizes (36 μm to 850 μm) to answer the following research questions:

1. Which laboratory-based particle size analysis method provides the most reliable measure of a particle size distribution?
2. Is there any systematic bias in any of the four laboratory-based particle size analysis techniques?
3. Are there any specific issues and considerations that need to be addressed when using any specific particle size analysis technique?
4. Is it possible to compare results of particle size analysis from different techniques, and do the results correlate?
5. How big are any statistically significant differences in the measured particle size distribution for a sample obtained using four different laboratory-based techniques?

2. Methodology

In this study, the techniques of LPSA, 2D automated image analysis, optical point counting, and XCT were used to evaluate eight samples composed of spherical silica particles. We measured the particle size distribution of each of the eight samples by mechanical sieving, and defined this range as the true measurement to compare the other four techniques against (Table 1). Spherical silica particle samples were used to evaluate the precise differences between analysis methods. Spherical silica particles were chosen over river or beach sediments as spherical silica particles eliminate any need to account for non-uniform particle shape and orientation that is common in geo-materials. All silica particles derive from the same bulk material, and are chemically identical, leaving the sieved (known) range as the only difference between samples. Each particle size analysis method used here is described in sections 2.1.1 to 2.1.4.

2.1. Sample Preparation

Bulk samples of spherical silica particles were obtained from the Wheelabrator Group. The spherical glass particles, as supplied, were heterogeneous in terms of particle size (Table 1); we refer to these as bulk samples. These bulk samples were refined into eight samples with narrow particle size ranges, via mechanical sieving of the bulk samples, adhering to the ASTM c136-06 standard method for sieving (Table 1). 1 kg of each bulk sample was placed into the top of a sieve stack and placed into an Endecott mechanical sieve shaker for five minutes. Each fraction was removed from the sieves, washed, dried, and stored in a sealed container. Samples were washed to remove fine material or dust, generated during sieving, that could skew the measured PSD. The particle size range of bulk samples and samples produced by mechanical sieving are reported in Table 1. Backscatter SEM images of all samples analysed in this study are presented in Figure 2.

Each technique outlined in this study uses a different mass of sample material and preparation technique to measure PSD. The differences in the minimum mass of sample required and the preparation techniques are detailed in sections 2.1.1 to 2.1.4.

2.1.1. Laser Particle Size Analysis (LPSA)

LPSA is a particle size analysis technique that was developed in the 1970s (Agrawal et al., 1991) and is a routine test method that is described by both ASTM (B822-20) and ISO (13322-1 2014) standards. In this study, a Beckman-Coulter LS13-320 particle size analyser with an aqueous liquid module (sometimes referred to as an ALM) was used. A schematic illustration of an LPSA device is shown in Figure 3. LPSA measures the PSD of a loose powder using the diffraction patterns of laser light, and the principle that particles of a defined size diffract light at a known angle, where the angle of diffraction is inversely proportional to particle diameter (Di Stefano et al., 2010). To measure PSD, a Fourier optic focused, parallel beam of monochromatic light, with wavelength of 750 nm passes through the sample cell. The diffracted light is focused onto an array of 126 photo-diode detectors placed at an angle of approximately 35 degrees from the optical axis (Beckman Coulter, 2011). The instrument measured the size of the suspended particles (equivalent spherical diameter; Figure 1), between 0.4 μm and 2000 μm , based on the Fraunhofer diffraction theorem, where an assumption is made that all particles are spherical, and no account is made for particle shape or orientation (de Boer et al., 1987; Blott et al., 2004). LPSA is a fast (approximately 5-10 minutes for each sample), non-destructive technique, and it is possible to recover the sample after analysis. Typically, LPSA requires less than 10 g of sample material per analysis.

The Beckman Coulter LS13-320 aqueous liquid module has been designed to work with loose particles, therefore no special sample preparation was required for spherical silica particles. The aqueous liquid module was filled with deionised water to avoid any contamination or charging of particles. To measure a PSD, first any material > 2000 μm was removed from a sample using a sieve, as this is the maximum particle diameter accepted by the LS13-320. If a sample contains organic material, this must be removed prior to analysis using hydrogen peroxide. It has been shown that the inclusion of organic material in a sample analysed by LPSA can skew the PSD towards the coarse fraction (Allen and Thornley, 2004), probably due to adhesion and clumping processes. Ultrasonic dissociation of a sample, either before or during analysis, was not employed in this study as it has been shown to skew the results towards the fine fraction (Ballard and Beare, 2013), likely due to destruction of particles. Each sample was slowly added into the loading chamber on the aqueous liquid module until the obscuration (a quantification of the amount of emitted laser light reaching the detector) was 10% (a range of 8-12% is suggested by Beckman Coulter (2011)). Particles were

circulated around a closed loop, ensuring that a representative measurement of the spherical particles was obtained (Figure 3). Analysis of a sample was carried out three times consecutively for a duration of one minute per analysis (three minutes total). Results were reported in volumetric percentages of the bulk sample that fall within each size bin. Size bins are spaced logarithmically between 0.4 μm and 2000 μm , and the logarithmic centre of each bin was used for the calculation of PSD descriptors. The results of the three independent analyses were exported, averaged, and input into GRADISTATv9.1 software in order to calculate PSD descriptors (Blott and Pye, 2001).

2.1.2. 2D automated Image Analysis by distance-watershed mapping

2D automated image analysis is a particle size analysis technique that is able to derive particle size and shape. Here, 2D automated image analysis was undertaken on SEM images. However, any type of photomicrograph can be used, as long as sufficient contrast exists between particles and background. Here, Backscatter Electron (BSE) images of polished resin blocks obtained using a Scanning Electron Microscope (SEM) were used for 2D automated image analysis. BSE images are high contrast, high spatial resolution images (e.g., nanometre scale), that allowed for precise 2D automated image analysis to be undertaken. Although not specific to SEM images, 2D automated image analysis is a standard test method described by ISO 13322-1:2014.

Spherical particles were made into polished resin blocks prior to SEM observation. 10 g samples of spherical particles were mixed with Struers EpoFix Resin in a 30 mm diameter mould, and placed under vacuum to remove air bubbles (0.17 bar for 30 minutes). Resin blocks were left to cure for 48 hours at room temperature. Resin blocks were removed from a mould and cut on a guide saw, where the blade and cutting fence are parallel. This was done to ensure particles were cut in a statistically random manner, and that the top and bottom of the blocks were parallel. Resin blocks were polished using a 4-stage workflow on a Struers LaboForce-100 automatic polisher (200 grit to 1 μm diamond solution). Polished blocks were coated with 10 nm of carbon, to prevent charging during SEM observation. A Zeiss Gemini 450 SEM, paired with Oxford Instruments Aztec software, was used to produce representative montage (stitched) images of the polished resin blocks. SEM imaging parameters used in this study are reported in Table 2. Montage images were imported into Fiji (Schindelin et al., 2012) and analysed using a 2D particle size analysis workflow. Images were first smoothed to remove noise by applying a bilateral filter (Thiede et al., 2019), as this has been suggested to preserve edges better than a median or Gaussian filter (Heim et al., 2016; Pashminehazar et al., 2016; Bernier et al., 2018), and converted into a binary image of particles and background. Particles in the binary image were separated and labelled using a 2D distance transform watershed algorithm within MorphoLibJ (Legland et al., 2016), which has been suggested to work

well for spherical particles (Behnsen et al., 2023). The parameters used for a distance transform watershed need to be selected appropriately, and human supervision is recommended, to avoid over- or under-segmenting particles (Behnsen et al., 2023). Any particles that were incorrectly separated were re-merged one-by-one, and clumped particles that were not correctly separated were split one-by-one and assigned a new label. This process prevents the introduction of artificial skew into the measured PSD. Any particles touching the edge of the montaged image were removed to avoid the measurement of non-whole particles. Labelled particles were analysed using the particle analyser tool within BoneJ (Domander et al., 2021). The results returned were: Ferret minimum (f_{min}), Ferret median (f_{med}), and Ferret maximum diameter (f_{max}) in micrometers, and surface area (μm^2) (Figure 1). Ferret minimum diameter is defined as the minimum measured diameter of a particle, and Ferret maximum diameter is defined as the maximum measure diameter of a particle (Figure 1). Surface area was converted into an equivalent circular diameter (μm) using equation 2, where A is the particle area (μm^2):

$$\text{Equivalent Circular Diameter} = \sqrt{\frac{4 \times A}{\pi}} \quad (2)$$

Al-Thyabat and Miles (2006) suggested that the measurements of primary importance for the comparison of PSD comparison are the equivalent circular diameter, and the shape factor.

$$\text{Shape factor} = \frac{f_{min}}{f_{max}} \quad (3)$$

Shape factor ranges from 0 to 1, where a perfect circle has a shape factor of 1 and a very elongate particle has a value approaching 0.

Particle circularity can also be calculated using equation 4 where A is the particle area (μm^2), and p is the particle perimeter length (μm):

$$\text{Circularity} = \frac{4\pi A}{p^2} \quad (4)$$

Circularity, like shape factor, ranges from 0 to 1. Where a perfect circle has a circularity of 1, and a very elongate particle has a value approaching 0.

2.1.3 Optical point counting by manual particle tracing

Optical point counting is a 2D particle size analysis technique that is able to return PSD and 2D particle shape measurements. Optical point counting can be performed using optical microscopy or SEM images of thin sections, by tracing the perimeter of the particles, or measuring the long and

short axis of particles. Here, optical point counting was undertaken on SEM images of polished resin blocks using PETROG optical point counting software, developed by Conwy Valley Systems, UK. The images used for optical point counting were the same images that are used for 2D automated image analysis. Polished resin blocks were produced, and BSE SEM image obtained using the method described in section 2.1.2. Montage images of silica particles were imported into PETROG, and a grid with >400 intersection points was overlain on the images. A grid was overlain on the image to reduce the chance of operator bias, and to introduce statistical randomness into the selection of particles measured during optical point counting. At each grid intersection point a particle was measured, until 300 measurements were recorded. If a particle was present, then the user manually traced the perimeter of the particle. This systematic method ensures that each particle was only counted once, reducing the amount of statistical error introduced into optical point counting (Middleton et al., 1985).

PETROG automatically calculated f_{min} , f_{max} , particle perimeter length, and the particle area. These measurements were used to calculate equivalent circular diameter (equation 2), shape factor (equation 3), and circularity (equation 4). 300 particle counts were chosen as it was determined by Mulholland and Jones (1968) that, for the calculation of mean grain size with >90% confidence even in a very poorly sorted sample, at least 270 particles are required to be measured.

2.1.4. X-ray Computed Tomography (XCT)

XCT is a non-destructive 3D image-based method that uses the transmission of X-rays through a sample to mathematically produce a 3D computed tomographic image. XCT can be undertaken on a loose powder, or a solid sample (e.g., rock chip or core plug). XCT was the only method analysed in this study that can produce measurements of 3D particle size, shape, and orientation. In addition, XCT analysis can be used to investigate the size and geometry of intraparticle porosity (Behnsen et al., 2023). Here, XCT analysis has been undertaken on loose particles contained within an X-ray transparent polyimide tube, mounted on to the head of a steel nail. The nail was clamped into a pin vice sample holder and inserted into a Zeiss Xradia Versa 620 Micro-CT scanner. A schematic illustration of an XCT device is shown in Figure 4. The scan conditions, and resulting voxel sizes, of the samples analysed in this study are detailed in Table 3. Raw data were processed in Fiji using a workflow based on the considerations suggested for particle size analysis using XCT by Behnsen et al. (2023). Raw XCT volumes were pre-processed using a non-local means filter, and converted to binary images of particles and background. Binarization was completed using a manual threshold, which here proved simple due the two-phase sample (silica particles and air). In more complex samples, with less consistent variation in contrast, the use of an image-based machine learning tool, such as

trainable WEKA segmentation (Arganda-Carreras et al., 2017), might yield improved results over a manual threshold (Wang et al., 2015). Particle edges were touching within the polyimide tube, and therefore were separated and individually labelled using a distance transform watershed algorithm. Particle separation relies on the assumption that the particles are separate and not fused or cemented together in any way (Behnsen et al., 2023). We employed a 3D distance transform watershed algorithm from the MorphoLibJ plugin for Fiji (Schindelin et al., 2012; Legland et al., 2016). An illustration of particle separation using a watershed algorithm can be found in Figure 6 of Behnsen et al. (2023). Particles in contact with the edge of the volume were removed to avoid the measurement of any non-whole particles.

Once particles were separated, they were measured to obtain a PSD. An overview of the various size and shape parameters employed in geoscience applications are illustrated in Figure 1.

Measurements of length (L), width (W), and breadth (B) are determined from the longest, shortest, and intermediate axes of the particles (Taylor et al., 2006). Particle volume was measured, using the number of voxels per particle, and converted into an equivalent spherical diameter using equation 5, where D is the particle diameter, and V is the particle volume:

$$D = \sqrt[3]{\frac{6V}{\pi}} \quad (5)$$

3D particle shape can also be quantified by calculating sphericity using equation 6, where Ψ is sphericity, V is particle volume, and SA is particle surface area:

$$\Psi = \frac{\pi^{\frac{1}{3}}(6V)^{\frac{2}{3}}}{SA} \quad (6)$$

To measure a particle accurately, it must be more than 3 voxels in diameter, otherwise there is a risk of confusing the particle with noise (Behnsen et al., 2023). To account for this, any particles smaller than 5 voxels in diameter (125 voxels in volume) were removed. Therefore, the minimum particle diameter measured using XCT ranged between 12 μm and 28 μm (i.e., 5 multiplied by voxel diameter (μm)). The number of particles that were measured ranged between 493 (sample 8) and 54,665 (sample 1) depending on restrictions of the field of view and the diameter of the particles.

2.2. Particle size distribution visualisation and descriptors

Raw data produced by each particle size analysis technique were input into GRADISTAT v9.1 in order to generate PSD descriptors (Blott and Pye, 2001). Here we used the geometric Folk and Ward (1957) calculations for particle size descriptors (mean, mode, and sorting), as these have been shown to provide the most robust measurements for the comparison of compositionally-variable

geological samples (Blott and Pye, 2001). Following the geometric Folk and Ward (1957) calculations, sorting has been calculated using equation 7, where D_x describes the diameter of which $x\%$ of the sample is smaller than:

$$sorting = \exp\left(\frac{\ln D_{16} - \ln D_{84}}{4} + \frac{\ln D_5 - \ln D_{95}}{6.6}\right) \quad (7)$$

A sample with a sorting value of: < 1.27 is very well sorted, 1.27 to 1.41 is well sorted, 1.41 to 1.62 is moderately well sorted, 1.62 to 2.00 is moderately sorted, and > 2.00 is poorly sorted. D_{10} , D_{50} , and D_{90} values have also been calculated. Particle size descriptors are reported geometrically (micrometers), rather than as logarithmic (Phi) units sometimes used in geoscience applications, because these SI units are recognised to be more applicable to a wide range of industries and disciplines (Blott and Pye, 2001). Visualisations of PSDs were produced within R statistical software (R Core Team, 2020) using the ggplot2 package (Wickham, 2016). Shape descriptors have been calculated for 2D automated image analysis, optical point counting, and XCT using equations 3, 4, and 6.

Normalised frequency similarity plots were produced to assess how data from each particle size analysis methods are distributed about the measured mean particle size. The produced plots are dimensionless and allow the comparison of data from different samples on one plot. Negative values indicate particle measurements smaller than the mean value, and positive values indicate particle measurements larger than the mean value. Similarity plots have been produced for XCT, optical point counting, and 2D automated image analysis. LPSA data cannot be plotted using this approach as measurements of individual particles are not reported.

Each particle size analysis method requires a different number of particle measurements to produce a representative PSD. To estimate the number of particles measurements required, the coefficient of variance for mean particle size has been calculated for each sample (where possible) using equation 8:

$$coefficient\ of\ variance = \frac{cumulative\ standard\ deviation}{cumulative\ mean} \quad (8)$$

For each particle size analysis technique, the mean coefficient of variance across the eight samples was calculated. Where the mean coefficient of variation plateaus, a sufficient number of particles have been measured to ensure that the mean particle size is statistically valid (Hinds et al., 2014). First order rate of change was used to determine stability of coefficient of variance.

To assess if the results from one particle size analysis technique correlate to the results of another technique, Pearson's correlation coefficients and p-values have been calculated in R using the 'rcorr' function as part of the 'Hmisc' package (Harrell Jr, 2019; R Core Team, 2020). Pearson's correlation

coefficients range from 1 to -1, where 1 is a strong positive correlation and -1 is a strong negative correlation. A value of 0 indicates that no correlation is present. P-values indicate the statistical significance of the correlation. For p-values <0.05 (*), the correlation is statistically significant. P-values <0.01 (**) indicate a very significant correlation and $p < 0.001$ (***) indicate an extremely significant correlation.

For techniques where individual particle measurements were reported (all techniques apart from LPSA), T-tests were performed to assess the similarity of the measured PSD. The T-tests performed were two-tailed, two-sample equal variance tests. T-tests were performed in R using the 't-test' function as part of the 'stats' package (R Core Team, 2020). For p-values less than 0.05, there is 95% confidence that there is a statistically significant difference between the PSDs. For p-values of less than 0.01, there is 99% confidence that there is a statistically significant difference between the PSD.

3. Data analysis and results

Presented here are the results of measuring eight different samples using the four-independent laboratory-based particle size analysis techniques. PSD descriptors (mean, mode, D10, D50, D90, and sorting) were calculated for each sample and method using the Folk and Ward method in GRADISTATv9.1 (Folk and Ward, 1957). In addition, the full PSD data are presented as frequency distribution, cumulative distribution, and similarity plots (Figure 5). We compare the results for each sample across all techniques, assessing the degree to which techniques agree. T-tests were used to assess the statistical significance of measured PSDs for individual samples. The Pearson's correlation coefficient was used to test the statistical significance between output from all techniques. Using the techniques capable of recording particle shape (e.g., length/width), the details of 2D versus 3D particle shape will be explored. Finally, the full morphology of particles, including the existence of particles with internal porosity will be analysed using XCT data.

3.1. Particle size distribution descriptors: mean, mode, D10, D50, D90, and sorting

PSD descriptors are shown in Table 4 and Figure 6. In the following section, we show how the measured PSD, and descriptors, compare for each sample and particle size analysis method.

Samples 1 and 2 ($<75 \mu\text{m}$): At small particle diameters, there is little variation in the mean, D50, and mode values measured by all techniques. All values measured using LPSA fall within the known sieved range. 2D automated image analysis, optical point counting, and XCT typically have the mean, mode, and D50 values within the sieved range, but the values for D10 and D90 rarely fall into the sieved range, especially for 2D automated image analysis and optical point counting. A larger range

in particle sizes is reported by 2D automated image analysis and optical point counting compared to LPSA and XCT, as shown by the sorting values for samples 1 and 2.

Samples 3, 4, and 5 (300 to 400 μm): At medium particle sizes, trends in the measured PSD, similar to those observed for smallest particles (samples 1 and 2), are recognised. For sample 4, the modal value for all techniques falls within the sieved range, but only the measurements of D50 for 2D automated image analysis and XCT are within the sieved range. All other descriptors are above or below the sieved 300 to 315 μm range. For sample 5, the values of modal particle size for LPSA, optical point counting, and XCT fall within the sieved range. The values of mean particle size and D50 produced using XCT also fall into the 315 to 400 μm range. For samples 3, 4, and 5, all other values are outside the sieved ranges. Descriptors measured using XCT most often fall into the range of sieved values for samples 3, 4, and 5, as the mean, modal, and D50 particle size are in the sieved range. No technique is able to measure D10 or D90 values within the sieved ranges for samples 3, 4, and 5. 2D automated image analysis in all cases produces the highest sorting values, whereas the smallest values are typically produced by XCT, except from sample 5. LPSA produces the smallest sorting values for sample 5 (1.194), however the values measured using XCT (1.244) are close to the LPSA measured values.

Samples 7 and 8 (> 600 μm): At large particle diameters, few descriptors are within the sieved ranges. For sample 7, only the D10 measurement for optical point counting and XCT fall in the sieved range. All other measurements are above the sieved range, with the measurements from 2D automated image analysis significantly greater than the other techniques. Optical point counting produces the smallest sorting values (1.046). However, the sorting values for XCT (1.063) are very close the optical point counting values. For sample 8, only the modal particle size value for XCT analysis is within the sieved range. All other values are outside the sieved range. All statistical values for LPSA and 2D automated image analysis are larger than the measurements produced by XCT. The measured values for optical point counting are smaller than the measured values for XCT. XCT produces the smallest sorting values for sample 8 (1.122).

Average sorting values were calculated for each analysis technique, over the whole particle size range (36 to 850 μm), to determine how constrained the measured PSD are for each technique. Lower average sorting values equate to smaller ranges in the measured PSD. Average sorting values are 1.233 for LPSA, 1.716 for 2D automated image analysis, 1.224 for optical point counting, and 1.191 for XCT.

3.2. Particle size distributions

Graphic displays of the PSD for all samples are shown in Figure 5. In all samples, LPSA detects few particles below 40 μm in diameter, in contrast to 2D automated image analysis and optical point counting. 2D automated image analysis and optical point counting have the largest tails, i.e., skew towards smaller particle sizes (Figure 5). This pattern is consistent across all samples analysed in this study. The large skew seen in the PSD of 2D automated image analysis and optical point counting is reflected in large sorting values (Table 4; Figure 6). Skew towards small particles for 2D automated image analysis is also associated with a spike in the number of the smallest particles measured (approximately 25 μm diameter). This pattern can be seen on the 2D automated image analysis line for all samples except 7 and 8 (Figure 5). For samples 3, 4, 5, 6, 7, and 8, LPSA shows a skew towards larger particles, where the pattern is exaggerated at larger particle sizes, reflecting the high mean, mode, D50, and D90 values that are recorded by LPSA (Table 4; Figure 6). Low sorting values of the XCT method are shown in Figure 5. The peak of the XCT curve (i.e., the highest frequency particle bin) is the one that is most likely to fall within the sieved range (red shaded area; Figure 5), reinforcing the observation that XCT most commonly has a modal particle diameter that is within the sieved particle size range.

Similarity plots reflect what can be seen on the frequency and cumulative distribution plots. The plots show that XCT is always the most evenly distributed about the mean, with optical point counting, and 2D automated image analysis skewed towards smaller values. SEM images analysis shows a larger skew towards smaller similarity values than optical point counting, particularly at larger particle sizes (samples 7 and 8). The average similarity plot (Figure 5) is calculated across all samples and particle size analysis methods. The average similarity plot shows that XCT and optical point counting perform to a similar degree. However, XCT has a higher frequency of measurements around the mean value, and shows fewer particles at both larger and smaller values than the mean, reflecting the smaller sorting values of XCT when compared to optical point counting.

3.3. Particle shape

In addition to PSD descriptors, 2D particle shape descriptors can be obtained from 2D automated image analysis and optical point counting using equations 2 and 4. 3D particle shape descriptors can be obtained from XCT using equation 5. LPSA is unable to produce any descriptors regarding particle shape as it is a bulk analysis technique; the Beckman Coulter LS13-320 does not report any measurements of individual particles, and therefore particle shape cannot be measured. Measurements of particle size and shape are reported in Table 7.

Sphericity values from XCT data are above 0.94, with a mean sphericity of 0.95. Using 2D automated image analysis, the calculation of circularity nearly always returns a value that is higher than the shape factor. The mean circularity value for 2D automated image analysis is 0.84 and the mean shape factor is 0.83. For optical point counting, the mean circularity is 0.95 and the mean shape factor is 0.86. The circularity value is higher than the shape factor value for both 2D automated image analysis and optical point counting.

3.4. Particle size distribution descriptors

T-test results are shown in Table 6 revealing that there is a > 95 % confidence that statistically significant difference exist between the measured PSDs for XCT, 2D automated image analysis, and optical point counting across all samples.

Pearson's correlation coefficients and p-values for each PSD statistic are shown in Table 5. Pearson's correlation coefficients (lower left half of the matrices) indicate if there is a correlation present. The p-values in Table 5 (upper right half of the matrices) show that a very, or extremely, statistically significant correlation exists between all particle size measurements, except for sorting values. For sorting, there is a very statistically significant correlation between LPSA, optical point counting, and XCT, but no statistically significant correlation between 2D automated image analysis and other techniques.

3.5. Coefficient of variance stability: number of particles required

The coefficient of variance in the mean particle size for XCT, 2D automated image analysis, and optical point counting are shown in Figure 7. Here, individual samples are shown in dotted lines and the mean coefficient of variance in a solid black line. The red dashed line indicates the point of stabilisation in the mean coefficient of variance, and therefore the number of particles that are required to be measured to stabilise the variance in mean particle size. Figure 7 shows that to stabilise the coefficient of variance in mean particle size, >250 particles are required for XCT, >350 particles are required for 2D automated image analysis, and >150 particles are required for optical point counting.

4. Discussion

4.1. Variation in measured particle size distribution

Figure 5 contains a graphical representation of PSD obtained across a range of particle diameters (36 to 850 μm) using four laboratory-based methods. It must be noted that the X-axes are different in each frequency distribution, and cumulative distribution plot, in order to display the range of

particle measured for each sample. Figure 5 shows that the PSDs agree (overlap) for some samples, but disagree for other samples. At all particle diameters, PSD data from both 2D automated image analysis and optical point counting are positively skewed (i.e., larger tails towards smaller particles). The positive skew identified in the distribution plots is reflected in the similarity plots. Positive skew is caused by the effect of stereology, or the slicing of particles through a random plane, and not through the particle centre, during the sample preparation stage. This known effect causes the measured diameter of a particle to be smaller than the maximum diameter of the particle, and is therefore not a true representation of the particle diameter (Sahagian and Prousevitch, 1998).

A different effect is apparent at larger particle diameters (samples 3 to 8). LPSA overestimates the number of large particles in a sample for samples with large particle diameters. This is likely due to the method by which particle diameter is calculated using the Mei and Fraunhofer theorems by LPSA (Ballard and Beare, 2013). As particles increase in diameter, the diffraction pattern of laser light has smaller spacing, and is therefore more difficult to detect. This effect leads to the bin widths produced by the Beckman Coulter LS13-320 to be logarithmically spaced between 0.375 μm and 2000 μm (increasing in width with increasing particle size). The pattern of LPSA overestimating the amount of coarse material has been supported by work by Ballard and Beare (2013) and Blott and Pye (2006). Blott and Pye (2006) used bi-modal mixtures of glass particles with the same density to investigate the manner of the overestimation of LPSA. They found that the overestimation of coarse material is exaggerated with increasing particle diameter, with up to a 300 % overestimation in the amount of coarse material present in the samples. Similarity plots cannot be produced for LPSA as the Beckman Coulter LS13-320 does not produce measurements of individual particles.

The similarity plots in Figure 5 highlight where the particle size analysis methods show a similar distribution, and where they do not. Here, they show that distributions produced using XCT and optical point counting are similar. XCT produces a more tightly constrained PSD than optical point counting, but the distribution of data around the mean is comparable. The large positive skew of 2D automated image analysis is highlighted by the similarity plots. This skew is apparent at all particle diameters.

4.2. Variation in the particle size distribution descriptors of each laboratory-based particle size analysis technique

We note similar trends in the PSD descriptors (Table 4; Figure 6) as we do in the PSD plots (Figure 5) for the range of samples analysed here. As particles increase in diameter, fewer statistical measurements are within the sieved ranges (Table 4; Figure 6). However, there are some consistent trends which should be noted.

XCT most commonly has statistical measurements with values within the sieved ranges, and sorting values from XCT are often the lowest of all the four techniques. XCT has the lowest average sorting values, suggesting that XCT particle size analysis is able to better contain a PSD across a range of particle diameters. Similar studies have been conducted on metal powders (Whiting et al., 2022). Here the authors find no significant difference between the PSD for XCT and 2D automated image analysis for particles in the size range of 20 to 76 μm . The samples analysed by Whiting et al. (2022) are equivalent to samples 1 and 2 from this study, where similar conclusions can be drawn about the correlation of XCT and 2D automated image analysis at small particle diameters. However, the trends observed by Whiting et al. (2022) are not apparent in our data at particle diameters greater than 150 μm (samples 3 to 8).

Values of average sorting support the observations that XCT produces the most tightly constrained PSD (1.191). Average sorting values for optical point counting and LPSA are close to XCT (1.224 & 1.233 respectively), but are larger due to the measured PSD being skewed. Optical point counting data are slightly positively skewed and LPSA data are slightly negatively skewed. 2D automated image analysis has the largest average sorting values (1.716), due to the large number of small particles measure. The measurement of small particles by 2D automated image analysis and optical point counting is an effect of stereology and the slicing of particles during sample preparation, causing the measured PSD to be positively skewed.

Pearson's correlation coefficients and p-values have been calculated to assess if there is a statistically significant correlation between the statistical measurement calculated from one PSA technique to another (Tables 5a to g). For mean particle size, modal particle size, D10, D50, and D90 there are statistically significant correlations between the values calculated for every technique. The values show that a strong linear relationship is present for all particle size measurements. The strong linear relationship, and low p-values, suggest that measurements of PSD obtained using one technique are comparable to the measurements generate using the other techniques.

For sorting, there is a statistically significant correlation between XCT and LPSA, and optical point counting. This suggests that the data from XCT, LPSA, and optical point counting techniques are comparable, and that results generated using one technique can be reasonably compared to those generated using a different technique. There is no significant correlation between the sorting values of 2D automated image analysis and other particle size analysis techniques. The sorting values of 2D automated image analysis do not show statistically significant correlation with other particle size analysis methods due to the effect of stereology artificially introducing skew, which subsequently affects values of D10 and D90 and sorting.

Table 5 shows that there is statistically significant correlation between the mean, mode, D10, D50, and D90 value for all particle size analysis in this study, suggesting that the comparison of data from one technique to another is possible. A Pearson's correlation coefficient of approaching one shows that there is a close to linear relationship between datasets although this good outcome does not mean that relationship is 1:1; a conversion factor may be required to relate data from one particle size analysis method to another (Hinds et al., 2014). The results from T-tests (Table 6) indicate that there is a significant difference between the measured PSDs for XCT, 2D automated image analysis, and optical point counting. The T-test results suggest that, although the statistical measured produced by each technique show a strong positive correlation, the comparison of data from one particle size analysis method to another is still challenging.

4.3. Advantages and disadvantages of each particle size analysis technique

Each particle size analysis technique has both advantages and disadvantages, particularly regarding the time involved in obtaining sample data. A summary comparing the preparation time, analysis time, and processing time for one sample using each technique from this study is shown in Table 8. This table highlights the total analysis time differences between the techniques and any additional data, besides a PSD and particle size descriptors, that can be obtained. Table 8 also includes additional advantages and disadvantages for each particle size analysis technique.

LPSA is a quick and repeatable technique for obtaining a PSD. It provides a consistent means of sample comparison, which provides sufficient data for the analysis of spatial or temporal variations in a dataset (Blott and Pye, 2006). We find that LPSA provides accurate particle size descriptor measurements for small particle (<300 μm), however the PSD produced by LPSA is skewed towards large particles. This agrees with prior work by Blott and Pye (2006), who found there to be significant differences in the PSD descriptors produced using LPSA and dry sieving, that increase in magnitude as particles became more irregular and elongate in shape. The results of particle size analysis data from LPSA must be compared carefully with data produced using a different particle size analysis method as only the PSD is reported and not the measurements of individual particles, limiting the calculation of some statistical measures (e.g. coefficient of variance in mean particle size).

When comparing PSD results generated using LPSA from different origins (e.g., different laboratories), care must be taken to establish exactly how the results were prepared and analysed. Clay-rich samples are commonly mixed with Sodium Hexametaphosphate, often referred to as Calgon, to aid the dispersion of clay particles. It has been found that, in particularly clay-rich samples, the use of Calgon can cause a bimodal PSD and lead to a dramatic increase in the amount

of fine material measured (Ballard and Beare, 2013). Another common practice is to subject a sample to sonication before analysis. The use of sonication has been suggested to skew to results of LPSA towards fine material, due to the breaking of particles along weak planes and the rounding of particles during collision with one another (Storti and Balsamo, 2010; Ballard and Beare, 2013). However, a recent study by Maithel et al. (2019) suggested that sonication of a sandstone for up to 20 minutes has no significant effect on the average particle size of a sample. Overall, understanding the exact sample preparation and analysis workflow is important for the meaningful comparison of LPSA results.

As well as particle size analysis, optical point counting can be used to determine the composition or mineralogy of particles in a thin section, with the user's aim typically being primarily to understand provenance or diagenesis. This method provides the user with numerical abundance data for the composition of a rock, and quantitative information about the size and shape of particles in the sample. Optical point counting is a slow method of obtaining a PSD, however manual measuring of particle perimeters it is particularly useful if particles are cemented or fragmented, and particle size is unlikely to be the only data that are derived (table 7). Here, we have used grid intersection points to introduce statistical randomness in the particles that have been measured. Where a user does not do this, there is a chance of artificially skewing a particle size distribution due to operator bias. Optical point counting can generate a wealth of data, such as mineralogy or grain coating clay coverage, that is not currently possible using other particle size analysis techniques (Van der Plas and Tobi, 1965; Wooldridge et al., 2019). However, the generation of additional data increases the analysis time for each sample.

2D automated image analysis is a simple method of particle size analysis that can be conducted on SEM images and optical photomicrographs. It is faster than traditional optical point counting, however less data can be simultaneously obtained. 2D automated image analysis is able to analyse thousands of particles in a very efficient manner. However, during a particle segmentation workflow, the user must monitor the process closely to ensure that particles are not over- or under-segmented, as this can introduce artificial skew into a dataset (Behnsen et al., 2023). Although not specific to particle size analysis, the use of a SEM can facilitate the collection of additional data such as chemical composition (SEM-EDS), and crystal orientation (SEM-EBSD). The use of an SEM to obtain representative images of a sample might not always be suitable, and sample preparation can prove time consuming (Table 8). It should also be noted that the samples used for 2D automated image analysis (or any sample made into a polished block or thin section) is non-recoverable.

XCT is the only particle size analysis method presented here that is able to produce 3D particle shape and particle orientation data. Depending on the size of the sample being analysed, and the required

resolution of the XCT scan, the sample analysis time can vary greatly. Here, all analysis times were less than 3 hours using laboratory-based XCT, where a maximum voxel size of 5.5 μm was achieved (Table 3). Scan times can be longer if the sample has a high X-ray absorbance, or a higher resolution is required. Sample size is a major limiting factor in XCT, and is determined by the X-ray absorbance and transmission of the X-ray beam through a sample. We have shown here that XCT is capable of measuring the PSD of particles in the $> 36 \mu\text{m}$ range, however the resolution of modern XCT systems is such that particles as small as 5 μm can be reliably scanned and segmented (Behnsen et al., 2023). A major advantage of XCT is that minimal sample preparation is required, and the sample can be fully recovered once analysis is complete. Therefore, it is suitable for a wide range of sample materials, and there is minimal risk of chemical alteration of a sample during preparation (e.g., alteration due to mixing with resin during polished resin block preparation). In addition to particle size analysis, XCT can also be used to investigate porosity, permeability, sedimentary structures and fabrics (Petri et al., 2020).

XCT is also capable of additional measurements such as preferential particle orientation, Zingg shape measurements (Zingg, 1935), and the size and distribution of intra-particle porosity (Behnsen et al., 2023). An example of these measurements is shown in Figure 8 for sample 3. The results of morphology analysis reveal all four Zingg classification are found within sample 3 and that 96.6% are spheres, 1.6% are disks, 0.4% are blades, and 3.4% are rods. The results also show that 39% of the particles in sample 3 have intra-particle (i.e., internal) porosity. For sample 3, the mean intra-particle porosity is 0.43%.

4.4. Comparing particle size distributions from different analysis methods

Each particle size analysis technique used in this study generated data using a different physical measurement, therefore comparison of data is challenging and needs to be conducted carefully. The quantitative outputs from each technique need to be chosen carefully, and some specific measurements can be more appropriate for comparing certain techniques (Whiting et al., 2022). Here, Pearson's correlation coefficients (Table 5) show statistically significant correlations exist mean, mode, D10, D50, and D90 values got all PSA methods. However, no statistically significant correlations are found between the sorting values produced by 2D automated image analysis and other PSA methods. Here, we have shown that LPSA overestimated the number of large particles in a sample and introduces a negative skew to the PSD. The opposite is apparent from 2D automated image analysis, which tends to overestimate the number of small particles in sample and introduce positive skew into the PSD. Therefore, the particle size descriptors used for the comparison of

techniques need to be considered carefully. Here, we suggest that measures of mean, mode, and D50 are the most appropriate descriptors to compare.

A longstanding problem in geoscience is the comparison of particle size descriptors obtained from 2D and 3D datasets. Subsequently, there have been numerous studies that aimed to establish conversion factors and derive the stereological relationship between 2D and 3D PSD. Theoretical conversion approaches have been proposed for idealised particles (e.g., spheres or ellipsoids) (Krumbein, 1935; Greenman, 1951; Packham, 1955; Sahu, 1966; Kellerhals et al., 1975; Johnson, 1994; Sahagian and Prousevitch, 1998; Jutzeler et al., 2012), while others developed empirical conversion factors, bypassing theoretical conversion factors (Friedman, 1958; Adams, 1977; Harrell and Eriksson, 1979; Kong et al., 2005; Jutzeler et al., 2012). A correction factor uses an equation that can convert a particle length measured in 2D to a more accurate representation that is equivalent to 3D, adjusting the measured PSD of a sample. However the applicability of conversion factors to sands and sandstones is limited (Weltje, 2002). The problem with using spherical particles to derive correction factors is that perfect spheres are not common in natural geo-materials, and therefore for non-spherical particles surface area or volume cannot be inferred from the measured cross section (Switzer, 2013). The number of times this topic has been approached reveals the difficulty of calculating a conversion factor that is consistent across a range of particle diameter and shapes. The calculation of a new set of correction factors is beyond the scope of this paper.

The advantage of collecting particle size information from thin sections, is that it can be collected along with mineralogical and rock fabric information that would be lost if a bulk technique such as sieving or LPSA were used. Thin section point count analysis is also a good method if the rock cannot be easily disaggregated due to cementation (Hinds et al., 2014). However, data collected from a 2D method such as optical point counting or 2D automated image analysis cannot be considered an accurate interpretation of 3D textures and fabrics within a sample, as a thin section is a cross-sectional slice and not a true representation of the sample in 3D (Hinds et al., 2014).

LPSA produces a smooth curve with tails that extend much further towards large particle than other techniques. It was suggested by Whiting et al. (2022) that the smoothness of curves produced by LPSA is an artefact a large sample size (more particle counted than other techniques) and that laser light can be refracted off multiple particle simultaneously, leading to the measurement of an artificial particle (multiple particles imaged as one particle) with a diameter that is larger than any particle in the bulk samples. Significantly, LPSA has the largest overestimation of D90 of any technique. Previous studies have suggested that comparing LPSA measurements with the f_{max} diameter generated using XCT analysis produces an acceptable correlation, but it will lead to an apparent overestimation of the PSD (Erdoğan et al., 2007). LPSA fundamentally assumes that all

particles are spherical, therefore non-spherical particles may have the longest edge measured, skewing the resulting PSD towards larger particles. The shape factor (termed “chunkiness” by Kaye et al. (1997)) of particles has been related to the skew of PSD measured using LPSA by Kaye et al. (1997). Kaye et al. (1997) demonstrated that at lower values of shape factor (less spherical), there is a larger range of particle sizes measured using LPSA, therefore the calculated values of sorting will be larger.

Here we have used a simplified sample set of spherical particles to determine how the differences between analysis techniques arise. Particles in geo-materials are not spherical and therefore it is important to understand how PSD techniques compare on more complex samples that contain non-spherical particles. Cheetham et al. (2008) conducted an extensive study with the aim of quantifying the PSD of sand-dominated sediments using sieving, LPSA, optical point counting, and X-ray attenuation. The authors found a strong correlation between LPSA and sieving, suggesting that the measured PSDs are equivalent. It is therefore suggested that the comparison of historical sieving data with modern LPSA data is valid (Cheetham et al., 2008). The data presented here only partly agrees with this conclusion. Samples 1 and 2 show an alignment of LPSA and sieving data, suggesting that, at particle diameters $\leq 75 \mu\text{m}$, data are comparable. However, at particle diameters $> 75 \mu\text{m}$ (samples 3-8 Figure 5) large particle diameters LPSA overestimates all PSD descriptors compared to the sieved interval, invalidating the comparison of data. This is due to the different measurements of particle diameter measured using each technique: sieving records the Ferret median diameter or breadth of a particle (Konert and Vandenberghe, 1997), whereas LPSA reports the equivalent spherical diameter of particles, based on the diffraction pattern of laser light (Di Stefano et al., 2010). As particles become less spherical and shape factor and sphericity decrease, the difference between a PSD measured with sieving and LPSA will likely increase (Kaye et al., 1997).

Optical point counting of thin sections and automated 2D image analysis to generate PSD are concepts that have been repeatedly examined (Krumbein, 1935; Greenman, 1951; Packham, 1955; Adams, 1977; Johnson, 1994; Cheetham et al., 2008; Maithel et al., 2019) but with variable outcomes. The results from these studies have determined that optical point counting and 2D automated image analysis underestimate mean particle diameter, and are skewed towards small particles when compared to LPSA (Maithel et al., 2019). The results shown in this study support the finding of previous authors that 2D measurements of PSD are skewed towards fine particle and tend to underestimate the mean particle diameter.

4.5. Statistically valid particle size distributions: number of particles required

The number of particles required to obtain a representative sample has been examined. Cheetham et al. (2008) undertook PSD analysis on SEM images using 100 particles per sample, and concluded that 100 particles are too few to be representative and therefore cannot be considered a valid method of particle size analysis. Alternatively, the number of particles required has been determined based on the sorting of the particles in a sample (Mulholland and Jones, 1968; Johnson, 1994). Mulholland and Jones (1968) suggested that to calculate mean particle size to within 0.1Φ with 90% certainty requires only 33 particles in a very well sorted sample, 100 particles in a moderately sorted sample, and 270 particles in a poorly sorted sample. It has also been suggested that up to 500 particles need to be measured to obtain statistically significant measurements of a PSD (Krumbein, 1935; Greenman, 1951; Friedman, 1958; Kellerhals et al., 1975). Instead of counting a pre-determined number of particles for every sample, Hinds et al. (2014) suggested that the variance in the mean particle diameter should be monitored, and when stable the number of particles required to obtain valid PSD descriptors has been reached. Following the methodology of Hinds et al. (2014) to calculate a mean variance for XCT, 2D automated image analysis, and optical point counting we have determined the minimum number of particle measurements needed to stabilise the variance in very well to moderately sorted samples (sorting values of < 1.27). For spherical particles, 250 particles are required to stabilise the variance from XCT (average sorting value; 1.191), 350 particles are required for 2D automated image analysis (average sorting value; 1.716), and 150 particles are required for optical point counting (average sorting value; 1.224). The number of particles determined here falls into the ranges previously suggested (Krumbein, 1935; Greenman, 1951; Friedman, 1958; Mulholland and Jones, 1968; Kellerhals et al., 1975). However it must be considered that the samples analysed in this study are very well sorted, and therefore the number of particles required to stabilise the variance in mean particle diameter is likely to increase as sorting values increase (more poorly sorted) (Mulholland and Jones, 1968)

5. Conclusions

We measured the particle size distribution of eight samples of spherical particles, with different size ranges, using four laboratory-based characterisation methods: Laser Particle Size Analysis (LPSA), 2D automated image analysis, optical point counting, and X-Ray Computed Tomography (XCT). We presented particle size distribution and distribution descriptors from the measured particle size distributions to investigate the correlation of measured particle size distributions from different methods.

1. LPSA is a bulk technique that is fast, cost-effective, and requires minimal sample preparation. However, the results are shown to overestimate the number of large particles, and introduce negative skew, due to the underlying principles of the Fraunhofer theorem. The data produced using LPSA contain no information regarding particle shape or morphology.
2. Optical point counting and 2D automated image analysis are 2D analysis methods conducted using photomicrographs or SEM images. Sample preparation leads to random slicing of particles, resulting in the majority of particle having a diameter that is less than their maximum. The effect of stereology positively skews the particle size distribution results. However, additional particle shape, morphology, and composition can be collected simultaneously.
3. XCT is the most reliable method of measuring a particle size distribution. XCT produced the smallest sorting values across the full range of particle diameters (36 to 850 μm); suggesting XCT constrains particle size distributions more accurately than LPSA, 2D automated image analysis, and optical point counting. Sample analysis and data processing times for XCT can be long, however quantitative measurements of 3D particle shape and intra-particle porosity can be made simultaneously to particle size; measurements not possible using LPSA, 2D automated image analysis, and optical point counting.
4. Statistically significant correlations exist between all techniques for mean and modal particle size, D10, D50, and D90 values. For sorting, a statistically significant correlation exists between LPSA, XCT, and optical point counting. However, there is no correlation between these techniques and values generated using 2D automated image analysis. This suggests that values mean, mode, D10, D50, and D90 values are comparable between different analysis methods. Values of sorting need to be compared with great care.

Data availability

Data will be made available on request.

Acknowledgements

This work was undertaken as part of the Chlorite Consortium at the University of Liverpool, sponsored by BP, Equinor, and DNO. The authors thank John S. Armstrong-Altrin for providing constructive comments. The authors gratefully acknowledge the Scanning Electron Microscope Shared Research Facility (SEM-SRF) at the University of Liverpool for their support and assistance in

this research. The authors also acknowledge the use of the SRF Zeiss Xradia Versa 620 at the University of Liverpool under the EPSRC strategic equipment grant number EP/V007610/.

Journal Pre-proof

References

- Adams, J., 1977. Sieve Size Statistics from Grain Measurement. *The Journal of Geology* 85, 209-227. <https://doi.org/10.1086/628286>
- Agrawal, Y.C., McCave, I.N., Riley, J.B., 1991. Laser diffraction size analysis. In: J.P.M. Syvitski (Ed.), *Principles, Methods and Application of Particle Size Analysis*. Cambridge University Press, Cambridge, pp. 119-128. <https://doi.org/10.1017/CBO9780511626142.012>
- Al-Thyabat, S., Miles, N.J., 2006. An improved estimation of size distribution from particle profile measurements. *Powder Technology* 166, 152-160. <https://doi.org/10.1016/j.powtec.2006.05.008>
- Ali, S.A., Clark, W.J., Moore, W.R., Dribus, J.R., 2010. Diagenesis and reservoir quality. *Oilfield Review* 22, 14-27.
- Allen, J.R.L., Thornley, D.M., 2004. Laser granulometry of Holocene estuarine silts: effects of hydrogen peroxide treatment. *The Holocene* 14, 290-295. <https://doi.org/10.1191/0959683604hl681rr>
- Arganda-Carreras, I., Kaynig, V., Rueden, C., Eliceiri, K.W., Schindelin, J., Cardona, A., Sebastian Seung, H., 2017. Trainable Weka Segmentation: a machine learning tool for microscopy pixel classification. *Bioinformatics* 33, 2424-2426. <https://doi.org/10.1093/bioinformatics/btx180>
- Ballard, T., Beare, S., Particle size analysis for sand control applications. In, *SPE European Formation Damage Conference & Exhibition*. 2013, Noordwijk, The Netherlands. OnePetro. <https://doi.org/10.2118/165119-MS>
- Beard, D.C., Weyl, P.K., 1973. Influence of Texture on Porosity and Permeability of Unconsolidated Sand. *AAPG Bulletin* 57, 349-369. <https://doi.org/10.1306/819a4272-16c5-11d7-8645000102c1865d>
- Beckman Coulter, 2011. LS 13 320 Laser Diffraction Particle Size Analyzer - Instructions for Use.
- Behnsen, J.G., Black, K., Houghton, J.E., Worden, R.H., 2023. A Review of Particle Size Analysis with X-ray CT. *Materials* 16, 1259. <https://doi.org/10.3390/ma16031259>
- Bernier, F., Tahara, R., Gendron, M., 2018. Additive manufacturing powder feedstock characterization using X-ray tomography. *Metal Powder Report* 73, 158-162. <https://doi.org/10.1016/j.mprp.2018.01.002>
- Blott, S.J., Pye, K., 2001. GRADISTAT: a grain size distribution and statistics package for the analysis of unconsolidated sediments. *Earth Surface Processes and Landforms* 26, 1237-1248. <https://doi.org/10.1002/esp.261>
- Blott, S.J., Croft, D.J., Pye, K., Saye, S.E., Wilson, H.E., 2004. Particle size analysis by laser diffraction. *Geological Society, London, Special Publications* 232, 63-73. <https://doi.org/10.1144/GSL.SP.2004.232.01.08>
- Blott, S.J., Pye, K., 2006. Particle size distribution analysis of sand-sized particles by laser diffraction: an experimental investigation of instrument sensitivity and the effects of particle shape. *Sedimentology* 53, 671-685. <https://doi.org/10.1111/j.1365-3091.2006.00786.x>
- Blott, S.J., Pye, K., 2012. Particle size scales and classification of sediment types based on particle size distributions: Review and recommended procedures. *Sedimentology* 59, 2071-2096. <https://doi.org/10.1111/j.1365-3091.2012.01335.x>
- Buckland, H.M., Saxby, J., Roche, M., Meredith, P., Rust, A.C., Cashman, K.V., Engwell, S.L., 2021. Measuring the size of non-spherical particles and the implications for grain size analysis in volcanology. *Journal of Volcanology and Geothermal Research* 415, 107257. <https://doi.org/10.1016/j.jvolgeores.2021.107257>
- Cadle, R.D., 1965. Particle size: Theory and industrial applications. Reinhold Publishing.
- Cheetham, M.D., Keene, A.F., Bush, R.T., Sullivan, L.A., Erskine, W.D., 2008. A comparison of grain-size analysis methods for sand-dominated fluvial sediments. *Sedimentology* 55, 1905-1913. <https://doi.org/10.1111/j.1365-3091.2008.00972.x>
- Church, M.A., McLean, D.G., Wolcott, J.F., 1987. River bed gravels: sampling and analysis. *Sediment transport in gravel-bed rivers*, 43-79.

- Church, M.J., 1978. Grain size and shape, *Sedimentology*. Encyclopedia of Earth Science. Springer Berlin Heidelberg, Berlin, Heidelberg, pp. 544-554. https://doi.org/10.1007/3-540-31079-7_104
- de Boer, G.B.J., de Weerd, C., Thoenes, D., Goossens, H.W.J., 1987. Laser Diffraction Spectrometry: Fraunhofer Diffraction Versus Mie Scattering. *Particle & Particle Systems Characterization* 4, 14-19. <https://doi.org/10.1002/ppsc.19870040104>
- Devarrewaere, W., Foqué, D., Heimbach, U., Cantre, D., Nicolai, B., Nuyttens, D., Verboven, P., 2015. Quantitative 3D shape description of dust particles from treated seeds by means of X-ray micro-CT. *Environmental science & technology* 49, 7310-7318. <https://doi.org/10.1021/acs.est.5b02250>
- Di Stefano, C., Ferro, V., Mirabile, S., 2010. Comparison between grain-size analyses using laser diffraction and sedimentation methods. *Biosystems Engineering* 106, 205-215. <https://doi.org/10.1016/j.biosystemseng.2010.03.013>
- Domander, R., Felder, A., Doube, M., 2021. BoneJ2 - refactoring established research software [version 2; peer review: 3 approved]. Wellcome Open Research 6. <https://doi.org/10.12688/wellcomeopenres.16619.2>
- Erdoğan, S.T., Garboczi, E.J., Fowler, D.W., 2007. Shape and Size of Microfine Aggregates: X-Ray Microcomputed Tomography vs. Laser Diffraction. *Powder Technology* 117, 53-63. <https://doi.org/10.1016/j.powtec.2007.02.016>
- Feret, L.R., 1930. La Grosseur des Grains des Matières Pulvérulentes. Eidgen. Materialprüfungsanstalt ad Eidgen. Technischen Hochschule, Premières Communications de la Nouvelle Association Internationale pour l'Essai des Matériaux, Groupe D.
- Folk, R.L., Ward, W.C., 1957. Brazos river bar: A study in the significance of grain size parameters. *Journal of Sedimentary Petrology* 27, 3-26. <https://doi.org/10.1306/74D70646-2B21-11D7-8648000102C1865D>
- Folk, R.L., 1966. A review of grain-size parameters. *Sedimentology* 6, 73-93. <https://doi.org/10.1111/j.1365-3091.1966.tb01572.x>
- Friedman, G.M., 1958. Determination of Sieve-Size Distribution from Thin-Section Data for Sedimentary Petrological Studies. *The Journal of Geology* 66, 394-416. <https://doi.org/10.1086/626525>
- Friedman, G.M., 1961. Distinction between dune, beach, and river sands from their textural characteristics. *Journal of Sedimentary Research* 31, 514-529. <https://doi.org/10.1306/74D70BCD-2B21-11D7-8648000102C1865D>
- Friedman, G.M., 1979. Differences in size distributions of populations of particles among sands of various origins: addendum to IAS Presidential Address. *Sedimentology* 26, 859-862. <https://doi.org/10.1111/j.1365-3091.1979.tb00979.x>
- Fripp, J.B., Diplas, P., 1993. Surface sampling in gravel streams. *Journal of Hydraulic Engineering* 119, 473-490. [https://doi.org/10.1061/\(ASCE\)0733-9429\(1993\)119:4\(473\)](https://doi.org/10.1061/(ASCE)0733-9429(1993)119:4(473))
- Gajjar, P., Styliari, I.D., Nguyen, T.T.H., Carr, J., Chen, X., Elliott, J.A., Hammond, R.B., Burnett, T.L., Roberts, K., Withers, P.J., Murnane, D., 2020. 3D characterisation of dry powder inhaler formulations: Developing X-ray micro computed tomography approaches. *European Journal of Pharmaceutics and Biopharmaceutics* 151, 32-44. <https://doi.org/10.1016/j.ejpb.2020.02.013>
- Greenman, N.N., 1951. The Mechanical Analysis of Sediments from Thin-Section Data. *The Journal of Geology* 59, 447-462. <https://doi.org/10.1086/625889>
- Harrell, J.A., Eriksson, K.A., 1979. Empirical conversion equations for thin-section and sieve derived size distribution parameters. *Journal of Sedimentary Research* 49, 273-280. <https://doi.org/10.1306/212f7711-2b24-11d7-8648000102c1865d>
- Harrell Jr, F.E., 2019. Package 'hmisc'. CRAN2018 2019, 235-236. <https://hbiostat.org/R/Hmisc/>
- Heim, K., Bernier, F., Pelletier, R., Lefebvre, L.P., 2016. High resolution pore size analysis in metallic powders by X-ray tomography. *Case Studies in Nondestructive Testing and Evaluation* 6, 45-52. <https://doi.org/10.1016/j.csndt.2016.09.002>

- Hinds, O., Duller, R.A., Walker, R.P., Wells, B.T., Worden, R.H., 2014. Enhanced two dimensional grain size analysis through the use of calibrated digital petrography. AAPG International Convention and Exhibition. Search and Discovery Article No. 41461.
- Houghton, J.E., Nichols, T.E., Griffiths, J., Simon, N., Utley, J.E.P., Duller, R.A., Worden, R.H., 2023. Automated Classification of Estuarine Sub-depositional Environment Using Sediment Texture. *Journal of Geophysical Research: Earth Surface* n/a, e2022JF006891. <https://doi.org/10.1029/2022JF006891>
- Jillavenkatesa, A., Dapkunas, S.J., Lum, L.-S.H., 2001. Particle size characterization. National Institute of Standards and Technology.
- Johnson, M.R., 1994. Thin section grain size analysis revisited. *Sedimentology* 41, 985-999. <https://doi.org/10.1111/j.1365-3091.1994.tb01436.x>
- Jutzeler, M., Proussevitch, A.A., Allen, S.R., 2012. Grain-size distribution of volcanoclastic rocks 1: A new technique based on functional stereology. *Journal of Volcanology and Geothermal Research* 239-240, 1-11. <https://doi.org/10.1016/j.jvolgeoes.2012.05.013>
- Kaye, B.H., Alliet, D., Switzer, L., Turbitt-Daoust, C., 1997. The Effect of Shape on Intermethod Correlation of Techniques for Characterizing the Size Distribution of Powder. Part 1: Correlating the Size Distribution Measured by Sieving, Image Analysis, and Diffractometer Methods. *Particle & Particle Systems Characterization* 14, 219-224. <https://doi.org/10.1002/ppsc.199700048>
- Kellerhals, R., Shaw, J., Arora, V.K., 1975. On Grain Size from Thin Sections. *The Journal of Geology* 83, 79-96. <https://doi.org/10.1086/628046>
- Konert, M., Vandenberghe, J., 1997. Comparison of laser grain size analysis with pipette and sieve analysis: a solution for the underestimation of the clay fraction. *Sedimentology* 44, 523-535. <https://doi.org/10.1046/j.1365-3091.1997.d01-38.x>
- Kong, M., Bhattacharya, R.N., James, C., Basu, A., 2005. A statistical approach to estimate the 3D size distribution of spheres from 2D size distributions. *GSA Bulletin* 117, 244-249. <https://doi.org/10.1130/b25000.1>
- Krumbein, W.C., 1935. Thin-Section Mechanical Analysis of Indurated Sediments. *The Journal of Geology* 43, 482-496. <https://doi.org/10.1086/624330>
- Krumbein, W.C., 1938. Size frequency distributions of sediments and the normal phi curve. *Journal of Sedimentary Research* 8, 84-90. <https://doi.org/10.1306/D4269008-2B26-11D7-8648000102C1865D>
- Legland, D., Arganda-Carreras, I., Andrey, P., 2016. MorphoLibJ: integrated library and plugins for mathematical morphology with ImageJ. *Bioinformatics* 32, 3532-3534. <https://doi.org/10.1093/bioinformatics/btw413>
- Maithel, S.A., Brand, L.R., Whitmore, J.H., 2019. A Methodology For Disaggregation and Textural Analysis of Quartz-cemented Sandstones. *Journal of Sedimentary Research* 89, 599-609. <https://doi.org/10.2110/jsr.2019.35>
- Mason, C.C., Folk, R.L., 1958. Differentiation of beach, dune, and aeolian flat environments by size analysis, Mustang Island, Texas. *Journal of Sedimentary Research* 28, 211-226. <https://doi.org/10.1306/74d707b3-2b21-11d7-8648000102c1865d>
- Middleton, A.P., Freestone, I.C., Leese, M.N., 1985. TEXTURAL ANALYSIS OF CERAMIC THIN SECTIONS: EVALUATION OF GRAIN SAMPLING PROCEDURES. *Archaeometry* 27, 64-74. <https://doi.org/10.1111/j.1475-4754.1985.tb00348.x>
- Mulholland, H., Jones, C.R., 1968. *Fundamentals of Statistics*. Springer US. <https://books.google.co.uk/books?id=BvIYvwEACAAJ>
- Packham, G.H., 1955. Volume-, Weight-, and Number-Frequency Analysis of Sediments from Thin-Section Data. *The Journal of Geology* 63, 50-58. <https://doi.org/10.1086/626225>
- Pashminehazar, R., Kharaghani, A., Tsotsas, E., 2016. Three dimensional characterization of morphology and internal structure of soft material agglomerates produced in spray fluidized bed by X-ray tomography. *Powder Technology* 300, 46-60. <https://doi.org/10.1016/j.powtec.2016.03.053>

- Petri, B., Almqvist, B.S.G., Pistone, M., 2020. 3D rock fabric analysis using micro-tomography: An introduction to the open-source TomoFab MATLAB code. *Computers & Geosciences* 138, 104444. <https://doi.org/10.1016/j.cageo.2020.104444>
- Pye, K., 1994. *Properties of sediment particles*. Blackwell: Oxford, Sediment Transport and Depositional Processes, 1-24 pp.,
- R Core Team, 2020. R: A language and environment for statistical computing. R Foundation for Statistical Computing, Vienna, Austria. <https://www.R-project.org/>.
- Rice, S., Church, M., 1996. Sampling surficial fluvial gravels; the precision of size distribution percentile sediments. *Journal of Sedimentary Research* 66, 654-665. <https://doi.org/10.2110/jsr.66.654>
- Sahagian, D.L., Proussevitch, A.A., 1998. 3D particle size distributions from 2D observations: stereology for natural applications. *Journal of Volcanology and Geothermal Research* 84, 173-196. [https://doi.org/10.1016/S0377-0273\(98\)00043-2](https://doi.org/10.1016/S0377-0273(98)00043-2)
- Sahu, B.K., 1966. Thin-Section Analysis Of Sandstones On Weight-Frequency Basis. *Sedimentology* 7, 255-259. <https://doi.org/10.1111/j.1365-3091.1966.tb01599.x>
- Schindelin, J., Arganda-Carreras, I., Frise, E., Kaynig, V., Longair, M., Pietzsch, T., Preibisch, S., Rueden, C., Saalfeld, S., Schmid, B., Tinevez, J.-Y., White, D.J., Hartenstein, V., Eliceiri, K., Tomancak, P., Cardona, A., 2012. Fiji: an open-source platform for biological-image analysis. *Nature Methods* 9, 676-682. <https://doi.org/10.1038/nmeth.2019>
- Simon, N., Worden, R.H., Muhammed, D.D., Utley, J.E.P., Verhagen, I.T.E., Griffiths, J., Wooldridge, L.J., 2021. Sediment textural characteristics of the Ravenglass Estuary; Development of a method to predict palaeo sub-depositional environments from estuary core samples. *Sedimentary Geology* 418, 105906. <https://doi.org/10.1016/j.sedgeo.2021.105906>
- Slotwinski, J.A., Garboczi, E.J., Stutzman, P.E., Ferraris, C.F., Watson, S.S., Peltz, M.A., 2014. Characterization of metal powders used for additive manufacturing. *Journal of research of the National Institute of Standards and Technology* 119, 460. <https://doi.org/10.6028/jres.119.018>
- Storti, F., Balsamo, F., 2010. Particle size distributions by laser diffraction: sensitivity of granular matter strength to analytical operating procedures. *Solid Earth* 1, 25-48. <https://doi.org/10.5194/se-1-25-2010>
- Switzer, A.D., 2013. Measuring and Analyzing Particle Size in a Geomorphic Context. In: J.F. Shroder (Ed.), *Treatise on Geomorphology*. Academic Press, San Diego, pp. 224-242. <https://doi.org/10.1016/B978-0-12-374739-6.00385-7>
- Taylor, M.A., Garboczi, E.J., Erdogan, S.T., Fowler, D.W., 2006. Some properties of irregular 3-D particles. *Powder Technology* 162, 1-15. <https://doi.org/10.1016/j.powtec.2005.10.013>
- Thiede, T., Mishurova, T., Evsevlev, S., Serrano-Munoz, I., Gollwitzer, C., Bruno, G., 2019. 3D Shape Analysis of Powder for Laser Beam Melting by Synchrotron X-ray CT. *Quantum Beam Science* 3, 3. <https://doi.org/10.3390/qubs3010003>
- Van der Plas, L., Tobi, A.C., 1965. A chart for judging the reliability of point counting results. *American Journal of Science* 263, 87-90. <https://doi.org/10.2475/ajs.263.1.87>
- Wang, Y., Lin, C.L., Miller, J.D., 2015. Improved 3D image segmentation for X-ray tomographic analysis of packed particle beds. *Minerals Engineering* 83, 185-191. <https://doi.org/10.1016/j.mineng.2015.09.007>
- Weltje, G.J., 2002. Quantitative analysis of detrital modes: statistically rigorous confidence regions in ternary diagrams and their use in sedimentary petrology. *Earth-Science Reviews* 57, 211-253. [https://doi.org/10.1016/S0012-8252\(01\)00076-9](https://doi.org/10.1016/S0012-8252(01)00076-9)
- Whiting, J.G., Garboczi, E.J., Tondare, V.N., Scott, J.H.J., Donmez, M.A., Moylan, S.P., 2022. A comparison of particle size distribution and morphology data acquired using lab-based and commercially available techniques: Application to stainless steel powder. *Powder Technology* 396, 648-662. <https://doi.org/10.1016/j.powtec.2021.10.063>

- Wickham, H., 2016. *ggplot2: Elegant graphics for data analysis*. Use R! Springer, Switzerland, 226 pp.,
- Wooldridge, L.J., Worden, R.H., Griffiths, J., Utley, J.E.P., 2019. How to quantify clay-coat grain coverage in modern and ancient sediments. *Journal of Sedimentary Research* 89, 135-146.
<https://doi.org/10.2110/jsr.2019.6>
- Zingg, T., 1935. Beitrag zur schotteranalyse. *Schweizerische Mineralogische und Petrographische Mitteilungen* 15, 38 - 140.

List of figures

Figure 1. Overview of the common particle size measurements used in geoscience. Length and width are commonly measured during optical point counting. Manual sieving records the width or Ferret-Min diameter. LPSA reports the diameter of a sphere of equal projection volume. XCT can report all measurements, as well as 3D particle shape measurements such as sphericity and orientation.

Figure 2. Backscatter SEM images of the samples analysed: a. sample 1 (35 to 65 μm), b. sample 2 (35 to 75 μm), c. sample 3 (150 to 180 μm), d. sample 4 (300 to 315 μm), e. sample 5 (315 to 355 μm), f. sample 6 (375 to 400 μm), g. sample 7 (600 to 630 μm), h. sample 8 (800 to 850 μm).

Figure 3. A schematic of an LPSA device. Particles are suspended in a fluid (de-ionised water) that circulated around the observation cell. Laser light passes through the analysis chamber and suspended particles refract the laser light. Larger particles produce smaller scattering angles than small particles. The angle of scattered light is measured by the detector. (Modified after Ballard and Beare 2013; Beckman Coulter 2011).

Figure 4. Schematic of a typical laboratory microfocus X-ray CT system. Shown here is the X-ray source, sample holder with sample (Kapton tube), and the detector. The detector on a Zeiss Xradia Versa 620 is a combination of the objective lens and camera. Source-sample and sample-detector distances affect image magnification. A series of projection images are captured while the sample is incrementally rotated over 360° , which is then reconstructed into the slice images that form the 3D data volume (Modified after Behnsen et al., 2023).

Figure 5. Frequency distribution (left) and cumulative distribution (centre), and similarity (right) plots for samples 1 to 8. XCT is shown with blue lines, LPSA with yellow lines, 2D automated image analysis with green lines, and optical point counting with red lines. The highlighted red area, bounded by dashed grey lines indicates the sieve range for each sample. Normalised frequency similarity plot (bottom) shows the average distribution produced by each particle size analysis technique. Both axes are dimensionless, allowing the comparison of all samples on one graph. LPSA cannot be plotted as measurements of individual particles are produced by the Beckman coulter LS13-320.

Figure 6. Visualisation of particle size distribution descriptors. The sieved range and symbols are coloured by sample: sample 1 (35 to 65 μm) = blue, sample 2 (65-75 μm) = orange, sample 3 (150 to 180 μm) = green, sample 4 (300 to 315 μm) = pink, sample 5 (315 to 355 μm) = brown, sample 6 (375 to 400 μm) = purple, sample 7 (600 to 630 μm) = red, and sample 8 (800 to 850 μm) = yellow. Data from each particle size analysis method has a different symbol: LPSA = stars, 2D automated image analysis = circles, optical point counting = squares, and XCT = triangles.

Figure 7. Coefficient of variance curves for XCT, 2D automated image analysis, and optical point counting. Variance is calculated using equation 7. Individual samples are shown in dotted lines, mean variance is shown in solid black lines. Red dashed lines indicate the number of particles after which the mean variance is stable.

Figure 8. Additional data that can be collected using XCT analysis. Shown here is an example from sample 3 (150 to 180 μm). Bottom: particles coloured by equivalent spherical diameter. Middle: particle coloured according to Zingg's shape classification (discs (I): purple, spheres (II): grey, blades (III): orange, rods (IV): blue). Top: particles with internal pores (particles perimeter in blue, intra-particle pores in red).

Table 1. Details of the samples analysed. Bulk samples of silica particles containing a large particle size distribution were sieved to extract narrow ranges of particle diameters. The bulk samples and the sieved fractions extracted from each bulk sample are detailed. Sieved fractions were used in the work here to analyse the measurement of a small, and known, grain size distribution using standard laboratory procedures.

Sample number	Bulk sample	Sieved Fraction
1	0 – 100 μm	36 – 65 μm
2	0 – 100 μm	65 – 75 μm
3	100 - 200 μm	150 – 180 μm
4	300 – 400 μm	300 – 315 μm
5	300 – 400 μm	315 – 355 μm
6	300 – 400 μm	355 – 400 μm
7	600 – 800 μm	600 - 630 μm
8	600 – 800 μm	800 – 850 μm

Table 2. SEM parameters used to image polished resin blocks on a Zeiss Gemini 450. All images and image montages were obtained using backscatter electron microscopy.

Sample number	Particle size range	Magnification	Beam Energy (kV)	Beam Current (nA)	Working distance (mm)	Pixel diameter (μm)
1	36 - 65 μm	150	20	2	10	0.75
2	65 - 75 μm	150	20	2	10	0.75
3	150 - 180 μm	80	20	2	10	1.4
4	300 - 315 μm	50	20	2	10	2.24
5	315 – 350 μm	50	20	2	10	2.24
6	375 – 400 μm	50	20	2	10	2.24
7	600 – 630 μm	50	20	2	9.5	2.24
8	800 – 850 μm	40	20	2	9.5	3

Table 3. XCT imaging parameters used for glass bead samples. Samples were scanned using a Zeiss Xradia Versa 620 X-ray Microscope.

Sample number	Particle size range	Objective	Binning	Exposure (s)	Number of projections	Source voltage (Kv)	Source wattage (W)	Beam filter	Pixel diameter (μm)
1	36 - 65 μm	4x	2	0.8	1601	60	6.5	Air	2.25
2	65 - 75 μm	4x	2	0.8	1601	60	6.5	Air	2.25
3	75 - 100 μm	4x	2	0.8	1601	60	6.5	Air	2.25
4	300 - 315 μm	4x	2	1.3	1601	80	10	Air	5.5
5	315 - 350 μm	4x	2	1.3	1601	80	10	Air	5.5
6	375 - 400 μm	4x	2	1.3	1601	80	10	Air	5.5
7	600 - 630 μm	4x	2	1.3	1601	80	10	Air	5.5 (stitched scans)
8	800 - 850 μm	4x	2	1.3	1601	80	10	Air	5.5 (stitched scans)

Table 4. particle size distribution statistics for all techniques and samples (LPSA = Laser Particle Size Analysis, 2D IA = 2D automated image analysis, OPC = optical point counting, and XCT = X-ray computed tomography). Statistical measurements were generated using GRADISTATv9.1. For sorting; vws = very well sorted, ws = well sorted, mws = moderately well sorted, ms = moderately sorted, and ps = poorly sorted following the geometrical Folk and Ward (1957) graphical measures.

Sample number	Particle size range	Technique	Mean	Mode	D10	D50	D90	Sorting
1	36-65 μm	LPSA	55.11	57.84	46.5	55.31	64.84	1.138 (ws)
		2D IA	63.5	75	31.74	70.17	88.42	1.477 (mws)
		OPC	55.84	65	43.09	56.76	68.49	1.192 (vws)
		XCT	59.26	65	50.27	59.77	68.94	1.166 (vws)
2	65-75 μm	LPSA	64.08	63.49	55.96	64.04	74.04	1.120 (vws)
		2D IA	60.55	95	23.03	74.86	96.86	1.730 (ms)
		OPC	63.34	65	48.27	64.77	76.23	1.199 (vws)
		XCT	68.5	75	57.03	69.03	77.87	1.133 (vws)
3	150-180 μm	LPSA	191.2	177.2	160.1	188.5	245.3	1.177 (vws)
		2D IA	113.6	165	33.27	135.4	176	1.829 (ms)
		OPC	157.4	175	106.9	164.4	189.8	1.255 (vws)
		XCT	154.9	175	97.61	166.7	184.2	1.262 (vws)
4	300-315 μm	LPSA	356.9	310	286.5	339.6	499.4	1.232 (vws)
		2D IA	232.7	305	55.83	308.4	436.3	2.065 (ps)
		OPC	268.1	305	187.7	282.9	335.8	1.263 (vws)
		XCT	293.7	305	193.7	307.6	338.9	1.226 (vws)
5	315-350 μm	LPSA	364.7	340.3	304	361	465.6	1.194 (vws)

		2D IA	190	295	55.98	220.6	469.3	2.278 (ps)
		OPC	304.3	345	223.3	319.6	355	1.196 (vws)
		XCT	315.3	345	191.5	334.8	360.9	1.244 (vws)
6	375-400 μm	LPSA	391.6	373.6	339.2	391.3	452.1	1.112 (vws)
		2D IA	292.5	425	106.2	347.2	471.5	1.760 (ms)
		OPC	304.6	325	237.7	312.2	372.3	1.195 (vws)
		XCT	374.2	375	331.6	375.1	400.9	1.169 (vws)
7	600-630 μm	LPSA	675	653.8	581.5	674.2	794.3	1.124 (vws)
		2D IA	843.6	885	580	888.9	976	1.234 (vws)
		OPC	644.1	645	609.5	644.1	681.7	1.046 (vws)
		XCT	653.8	635	617.3	648.2	720.3	1.063 (vws)
8	800-850 μm	LPSA	1008.7	949.4	791.3	972.6	1413.9	1.246 (vws)
		2D IA	930.1	735	651	977.5	1179	1.316 (ws)
		OPC	741.2	755	633.3	739.4	903.3	1.140 (vws)
		XCT	881.8	845	686	874.6	968.5	1.122 (vws)

Table 5. Results of Pearson’s correlation coefficient and p-values for the particle size distribution statistics of all samples. The value of a Pearson’s correlation coefficient ranges from 1 to -1, where 1 is a strong positive correlation and -1 is a strong negative correlation. A value of 0 indicates that no correlation is present. P-values indicate the statistical significance of the correlation. For p-values <0.05 (*), the correlation is statistically significant. P-values <0.01 (**) indicate a very significant correlation and p <0.001 (***) indicate an extremely significant correlation. LPSA = Laser Particle Size Analysis, 2D IA = 2D automated image analysis, OPC = optical point counting, and XCT = X-ray computed tomography.

x	mean.LP SA	mean. 2D IA	mean.O PC	mean.X CT	x	mode.LP SA	mode. 2D IA	mode.O PC	mode.X CT
mean.LP SA	x	0.000* **	0.000** *	0.000** *	mode.LP SA	x	0.002* *	0.000** *	0.000** *
mean.2 D IA	0.954	x	0.000** *	0.000** *	mode.2 D IA	0.913	x	0.000** *	0.001**
mean.O PC	0.984	0.98	x	0.000** *	mode.O PC	0.986	0.955	x	0.000** *
mean.X CT	0.994	0.969	0.991	x	mode.X CT	0.987	0.94	0.989	x
x	d10.LPS A	d10.2D IA	d10.OP C	d10.XC T	x	d50.LPS A	d50.2D IA	d50.OP C	d50.XC T
d10.LPS A	x	0.001* *	0	0	d50.LPS A	x	0.000* **	0.000** *	0.000** *
d10.2D IA	0.916	x	0	0	d50.2D IA	0.964	x	0.000** *	0.000** *
d10.OPC	0.973	0.967	x	0	d50.OPC	0.986	0.981	x	0.000** *
d10.XCT	0.977	0.956	0.989	x	d50.XCT	0.993	0.971	0.991	X
x	d90.LPS A	d90.2D IA	d90.OP C	d90.XC T	x	sort.LPS A	sort.2 D IA	sort.OP C	sort.XC T
d90.LPS A	x	0.000* **	0.000** *	0.000** *	sort.LPS A	x	0.593	0.002**	0.006**
d90.2D IA	0.966	x	0.000** *	0.000** *	sort.2D IA	0.225	x	0.252	0.085
d90.OPC	0.982	0.996	x	0.000** *	sort.OPC	0.907	0.46	x	0.000** *
d90.XCT	0.977	0.996	0.994	X	sort.XCT	0.857	0.644	0.948	x

Table 6. T-test results for Samples 1 to 8. T-tests have been performed on XCT, SEM image analysis, and Point Counting data. T-tests cannot be performed on LPSA data as the Beckman Coulter LS13-320 does not produce measurements of individual particles. For p-values less than 0.05, there is 95% confidence that there is a statistically significant difference between the particle size distributions. For p-values of less than 0.01, there is 99% confidence that there is a statistically significant difference between the particle size distributions. 2D IA = 2D automated image analysis, OPC = optical point counting, and XCT = X-ray computed tomography.

36-65um	XCT - 2D IA	XCT - OPC	2D IA - OPC
T-statistic	0	0.01	0
Confidence level	100	98.63	100
65-75um			
T-statistic	0	0	0
Confidence level	100	99.99	100
150-180um			
T-statistic	0	0.01	0.09
Confidence level	99.99	98.96	91.43
300-315um			
T-statistic	0	0	0
Confidence level	100	100	100
315-350um			
T-statistic	0	0.05	0
Confidence level	100	95.42	100
375-400um			
T-statistic	0	0	0
Confidence level	100	100	100
600-630um			
T-statistic	0	0	0
Confidence level	100	99.99	100
800-850um			
T-statistic	0	0	0
Confidence level	100	100	100

Table 7. Results of shape analysis for XCT, 2D automated image analysis, and optical point counting. Details of the calculations are in equations 2 and 3. Circularity, sphericity, and shape factor range between 0 and 1, where a perfect sphere/circle has a value of 1. 2D IA = 2D automated image analysis, OPC = optical point counting, and XCT = X-ray computed tomography.

Sample	Sphericity from XCT	2D IA shape factor	2D IA circularity	OPC shape factor	OPC Circularity
36-65 μm	0.96	0.86	0.87	0.87	0.94
65-75 μm	0.94	0.82	0.84	0.85	0.93
150-180 μm	0.95	0.83	0.85	0.84	0.95
300-315 μm	0.95	0.76	0.84	0.84	0.94
315-355 μm	0.95	0.79	0.75	0.86	0.95
375-400 μm	0.97	0.89	0.86	0.87	0.99
600-630 μm	0.97	0.85	0.85	0.88	0.88
800-850 μm	0.94	0.8	0.84	0.84	0.84

Table 8. Summary of the advantages and disadvantages for each particle size analysis method. The data include sample preparation time, analysis time, data processing time, and any additional data that can be collected. LPSA = Laser Particle Size Analysis, 2D IA = 2D automated image analysis, OPC = optical point counting, and XCT = X-ray computed tomography.

Technique	Sample preparation method	Sample preparation time	Sample analysis time	Data processing time	Total time	Additional data	Advantages	Disadvantages
LPSA	Disaggregation and removal of organic material	0-1 hours typically.	10 minutes	5 minutes	<1 hour	N/A	Reliable method to assess spatial and temporal variation in a dataset	Produces different particle size distributions to other common techniques.
		Up to 48 hours						Results can be influenced by sample preparation (e.g. mixing with Calgon, or the use of sonication).
2D IA	Thin section or polished block production	4 hours	1 hour	0.5 hour	6 hours	2D particle shape	Large datasets (e.g. whole thin sections) can be analysed quickly. Not subject to user bias.	Time consuming sample preparation. Data can be artificially skewed during particle separation

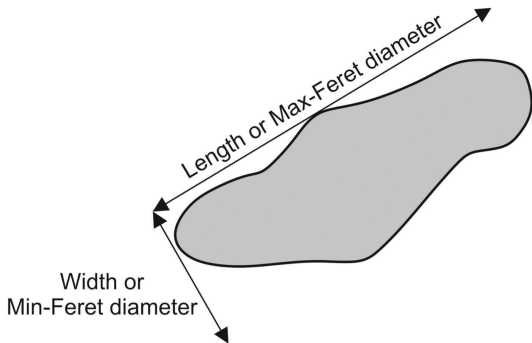
OPC	Thin section or polished block production	4 hours	3 hours	5 minutes	7 hours	2D particle shape. Mineralogy.	Sample composition can be determined – use in provenance and diagenesis studies.	Time consuming
XCT	Place loose sample in Kapton tube, or mount solid sample to a nail	0.5 hours	1-3 hours	1 hour	5 hours	3D particle shape. Porosity and Intraparticle porosity. Grain fabrics/preferential orientation.	Not subject to the effect of stereology.	Lower particle size limited to ~12 μm .

Declaration of interests

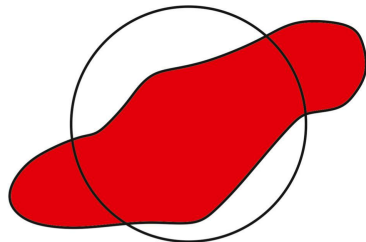
The authors declare that they have no known competing financial interests or personal relationships that could have appeared to influence the work reported in this paper.

The authors declare the following financial interests/personal relationships which may be considered as potential competing interests:

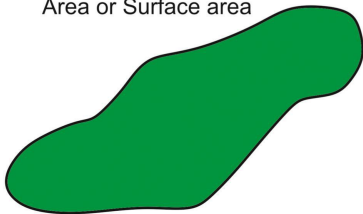
Journal Pre-proof



Diameter of a sphere of equal projection volume/area as the particle



Area or Surface area



Perimeter length

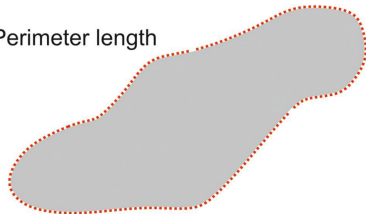


Figure 1

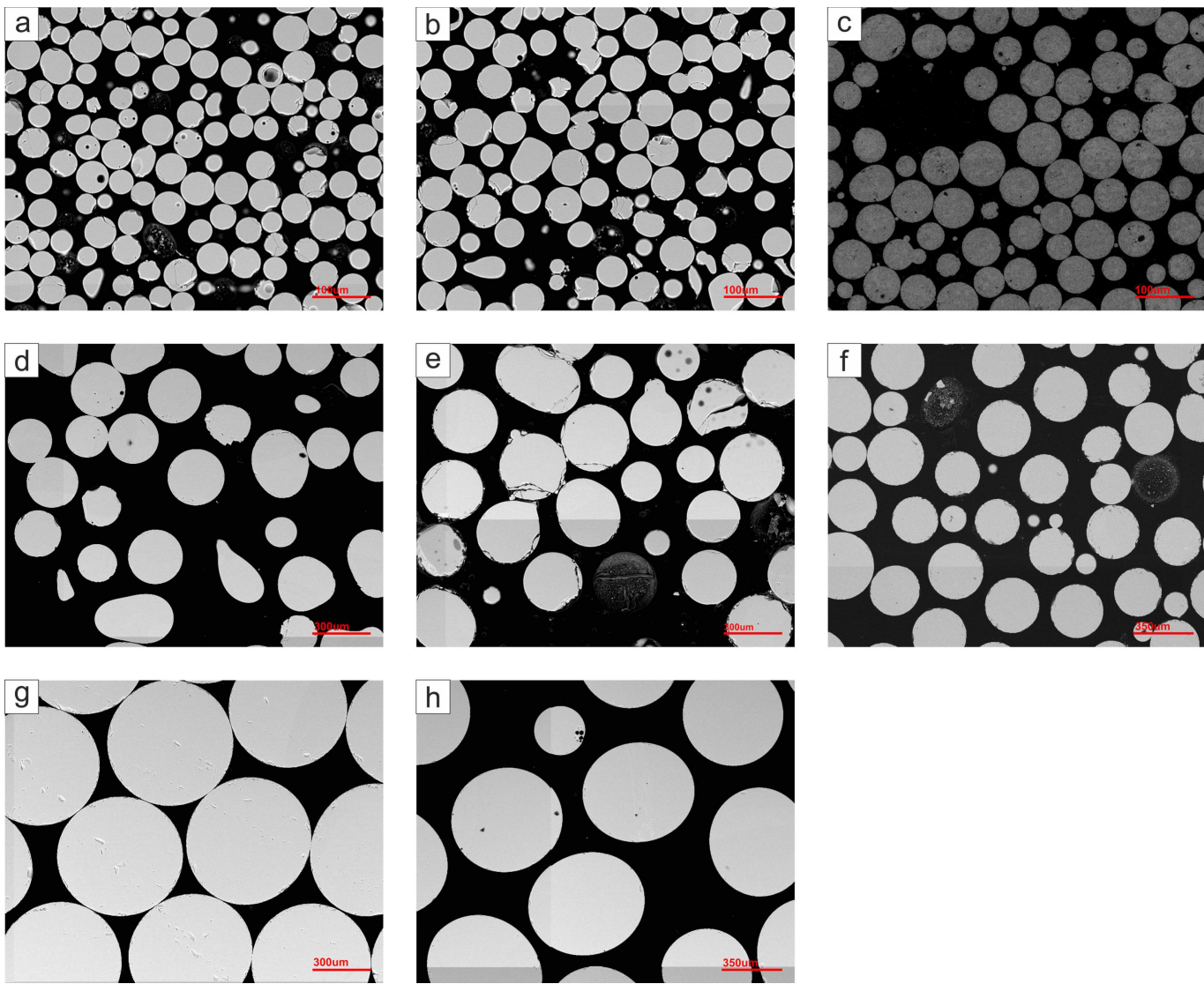


Figure 2

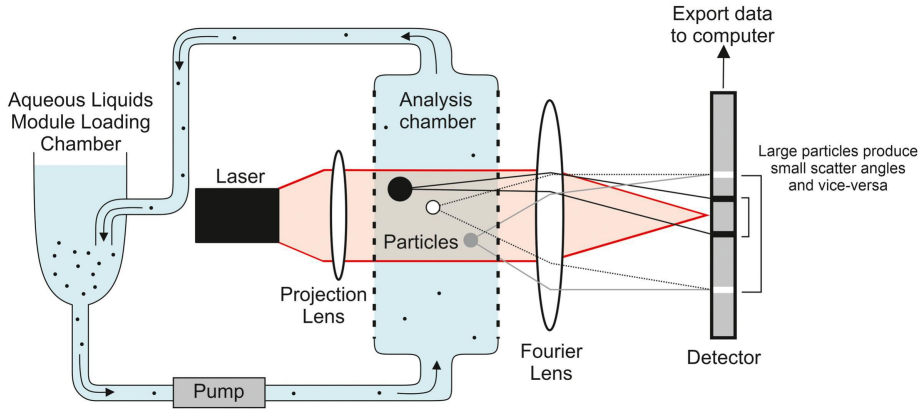


Figure 3

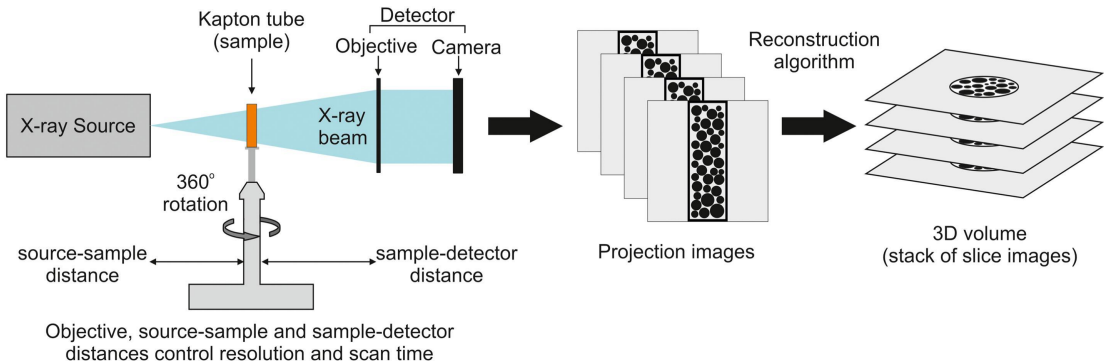


Figure 4

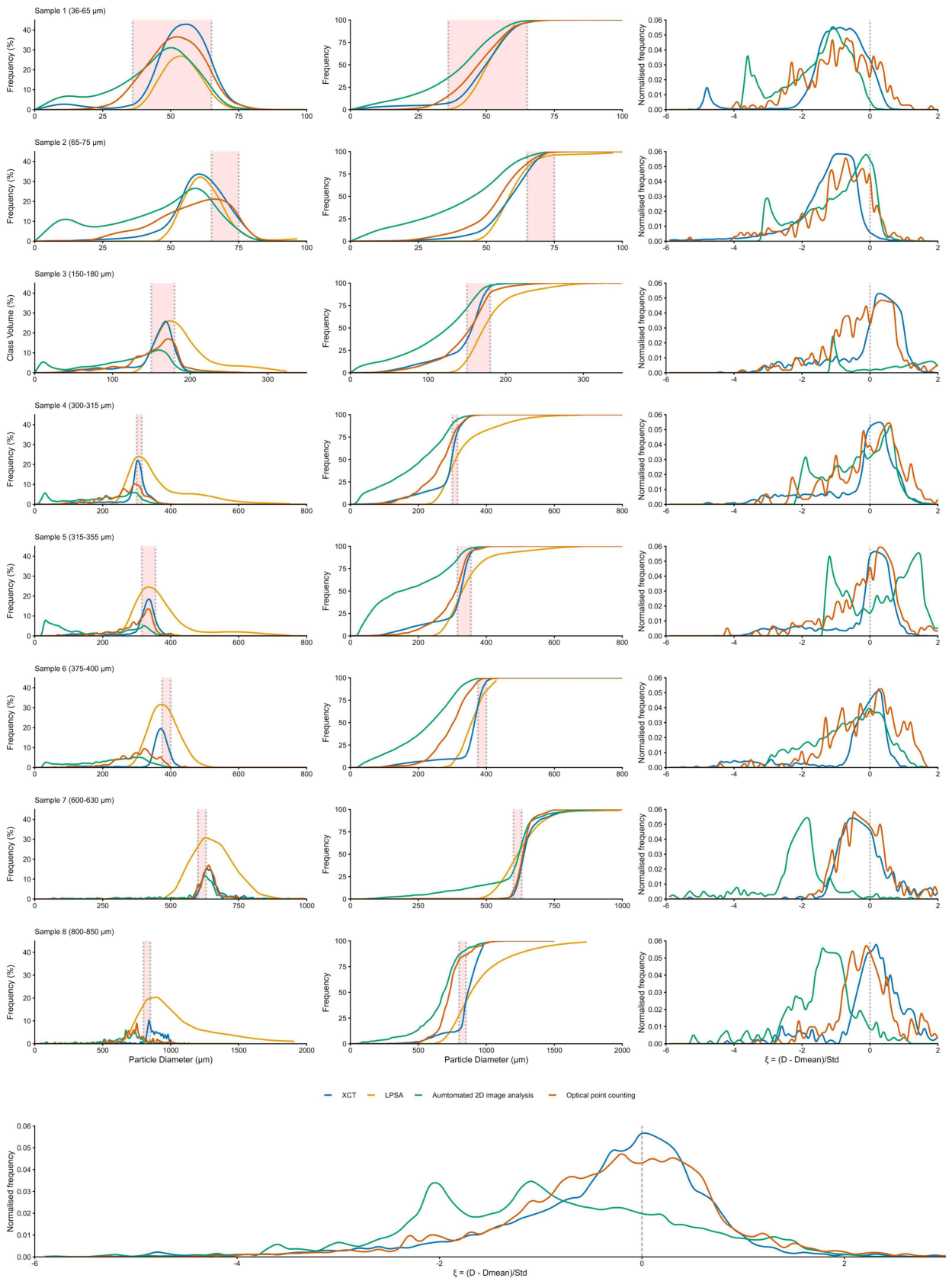


Figure 5

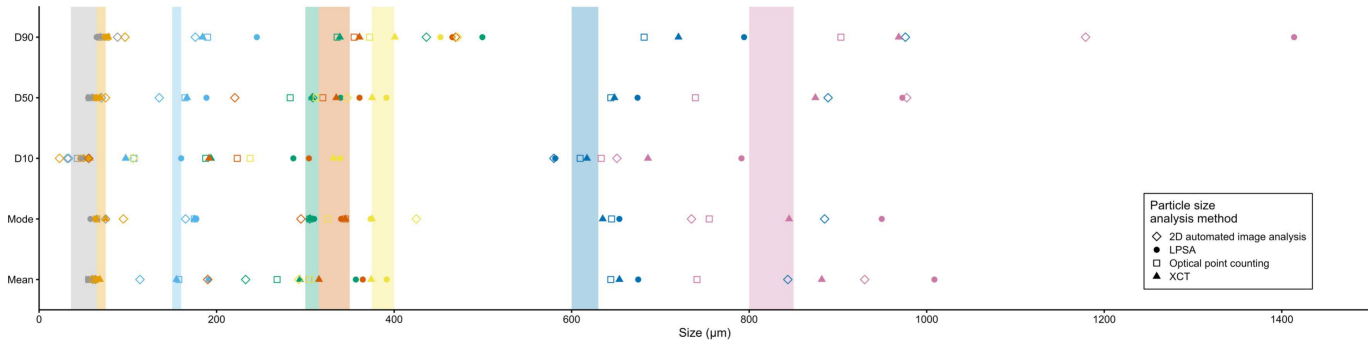


Figure 6

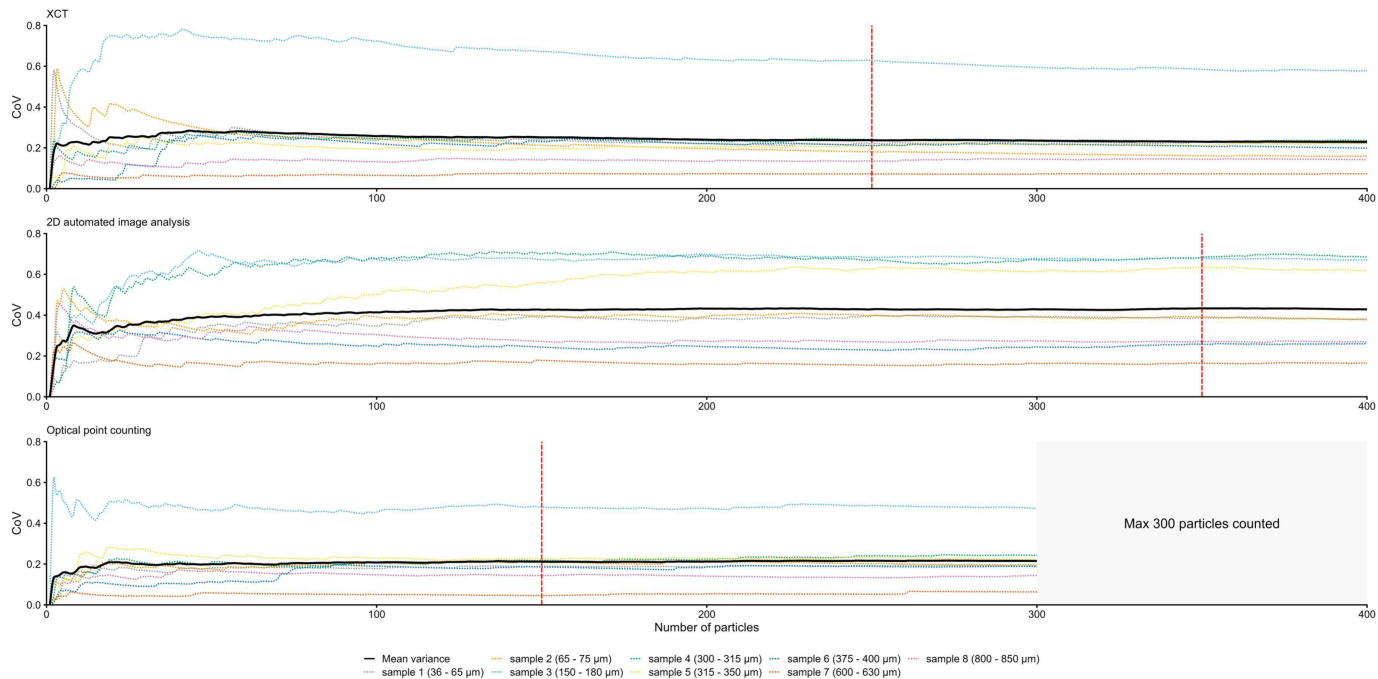


Figure 7

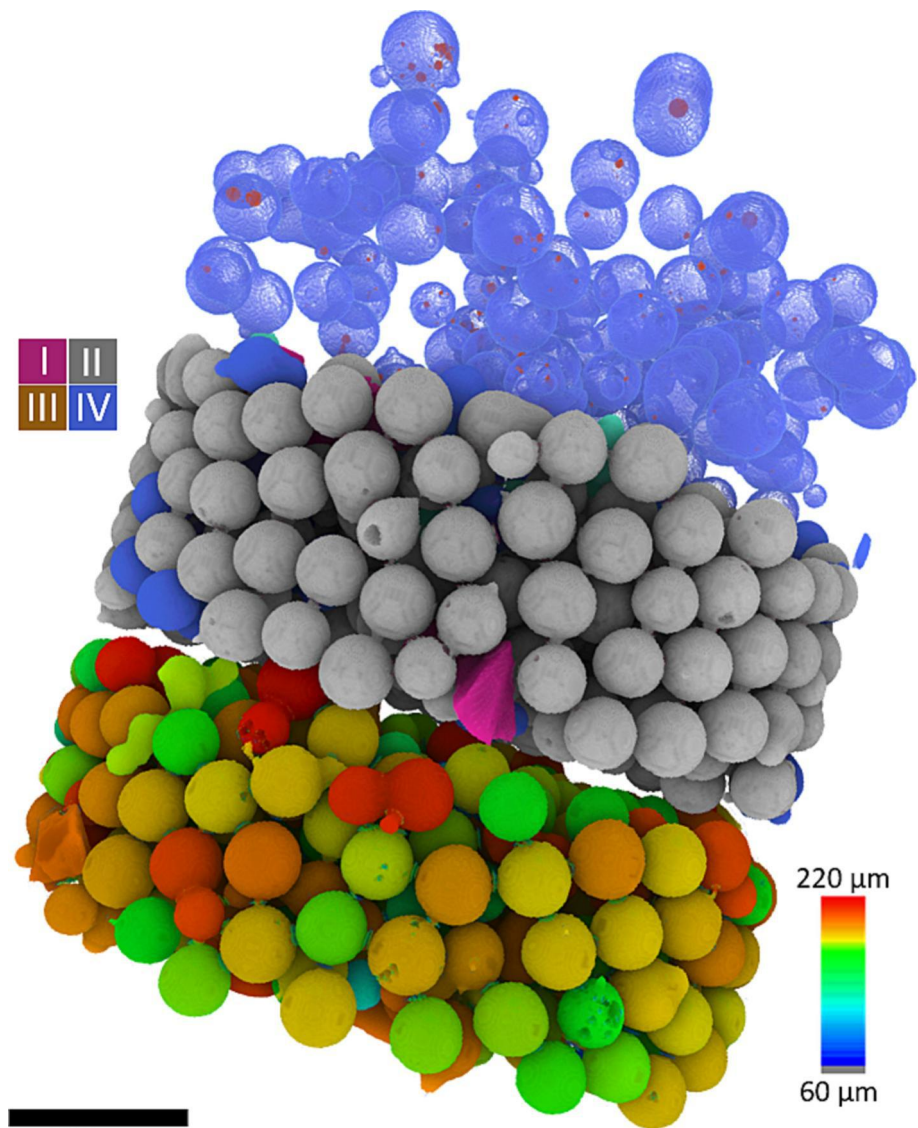


Figure 8